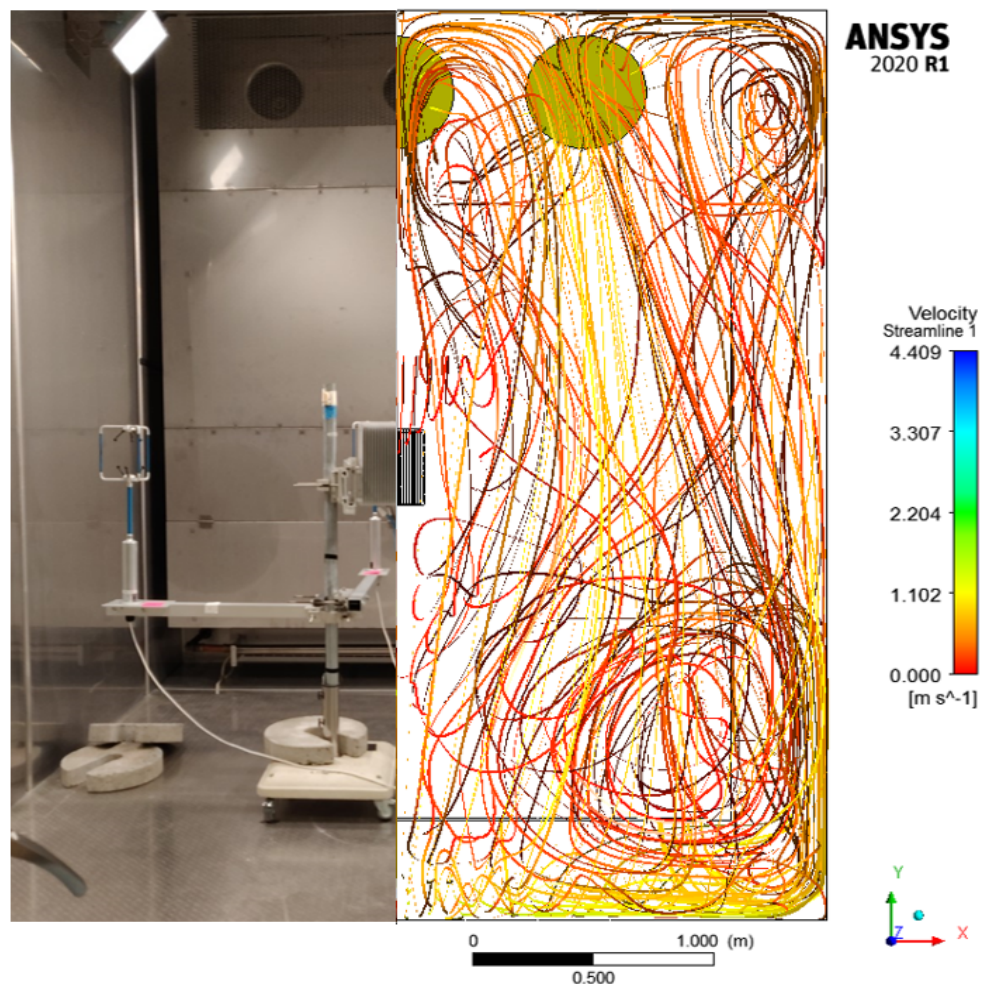


# Master thesis - Towards a virtual climate chamber

Yuvarajendra Anjaneya Reddy



**ERICSSON**



# Master thesis - Towards a virtual climate chamber

---

**Yuvarajendra Anjaneya Reddy**

Academic supervisor: **Roland Gårdhagen**,  
Senior lecturer  
IEI, Linköpings Universitet

Industrial supervisor: **Mireia Altimira**, PhD,  
Senior Developer Thermal Design  
Ericsson, Blåfjällsgatan 4, Stockholm

Examiner: **Matts Karlsson**,  
Professor  
IEI, Linköpings Universitet

# Abstract

For each generation of electronic equipment there is a trend towards higher power densities. Increased heat generation is an undesired consequence that the thermal design unit in a company must handle. The goal of thermal design engineer/unit is to utilize the same volume to more efficiently transfer more heat from the equipment. This can be done by exploring more complex and advanced heat sink geometries, optimizing the fin shapes and so on. The new prototypes developed will be tested for their reliability and endurance in special chambers called climate chambers, that simulate desired environments. The measurements by thermal design teams in these kind of climate chambers are mainly of outdoor products, whose cooling is based on natural convection. Forced cooling using fans is optional for these outdoor products.

The climate chambers in general provides temperature measurement as the output to the analysis, though there are other important parameters that define the operational functionality of an equipment. The ability to visualize the flow characteristics during the process of testing is a valuable aid in the design process. A virtual/CFD form of the physical climate chamber (CC) would empower the design process, while alleviating the usage of the climate chambers for such analyses. CFD offers a wide range of capabilities that lets the user change the boundary conditions with great ease compared to that of the experimental setup.

The numerical model developed in this thesis project provides results, that help in understanding the physics involved in fluid flow inside the physical climate chamber. Turbulence quantification of the flow is the main aim of this thesis project, which would be resourceful in future works. Experiments are conducted inside the climate chamber, in order to aid the construction of numerical model as well as serve as source of validation for the numerical results. Laminar transient case simulations are preferred over use of any turbulence models, to limit any kind of predictions made by these turbulence models. Integral length scales and turbulence intensities are compared and reason for discrepancies are addressed.

The results from the comparisons show that, the numerical model emulates physics of actual flow inside the climate chamber. However, there are many factors that directly affect the results, making it difficult to precisely quantify the error, within the time period of this thesis project.

**Keywords:** Climate chamber, Computational fluid mechanics, turbulence, thermal design, turbulence spectra, Energy Density Spectrum, Integral length scales, Turbulent intensity

# Acknowledgements

I would like to express my sincere gratitude towards my mate, **Javier Arroyo Molina**, M.Sc Chemical Engineering, from KTH University, Stockholm, for being a part of this thesis and handling the experimental section of this thesis project.

I would also like to give my utmost gratitude to my company supervisor at Ericsson AB, **Mireia Altimira**, PhD for their guidance throughout the thesis work and their help with the administrative aspect. I am particularly thankful to **Stevin Van Wyk**, PhD, Ericsson AB, for his inputs and helping me understand the turbulence modelling in a better way. It wouldn't be fair if I'd not mention the enormous amount of supervision, motivation and guidance I received from my industrial supervisors, throughout the thesis period amid the huge corona virus fuss. I consider myself to be lucky enough to be tutored under them.

I am also thankful to my university supervisor, **Roland Gårdhagen**, Senior lecturer, IEI, Linköpings University for his timely guidance and valuable comments during this project course.

I thank Ericsson AB for providing computational resources for CFD simulations and its administrative staff for speedy resolutions of my queries. Finally, I wish to thank my family for their love and support without which I would never have enjoyed this opportunity. And I would never fail to mention the moral support I have received from my juniors at Linköpings University and friends from my karma-bhoomi, Nandagudi, India.

Yuvarajendra Anjaneya Reddy

# Nomenclature

## Abbreviations and Acronyms

Abbreviation	Meaning
CAD	Computer-aided Design
CAE	Computer-aided Engineering
CC	Climate Chamber
CFD	Computational fluid dynamics
CFL	Courant-Friedrichs-Levy
DES	Detached Eddy Simulations
DNS	Direct Numerical Simulation
HTC	Heat Transfer Coefficient
LES	Large-Eddy Simulations
LiU	Linköping University
RANS	Reynolds Averaged Navier-Stokes
RMS	Root Mean Square
RNG	Re-Normalisation Group
SAS	Scale Adaptive Simulations
SGS	Sub Grid Scale
SRS	Scale Resolving Simulations
SST	Shear Stress Transport
TKE	Turbulent Kinetic Energy
tSST	Transitional Shear Stress Transport
URANS	Unsteady Reynolds Averaged Navier Stokes

## Dimensionless Numbers

Abbreviation	Description
$E$	Spectral Energy
$I_{in}$	Turbulent Intensity at the inlet
Gr	Grashoff's number
Pr	Prandtl Number
Ra	Rayleigh Number
Re	Reynolds number
$U$	Average velocity
$y^+$	Normalized wall distance

## Latin Symbols

Symbol	Description	Units
$\sigma$	Standard deviation	-
$\rho$	Density	$[Kgm^{-3}]$
$\mu$	Dynamic Viscosity	$[Kgm^{-1}s^{-1}]$
$\tau$	Wall Shear Stress	$[Nm^{-2}]$
$\ell$	Length scale	$[m]$
p	Pressure	$[Pa]$
t	Time	$[s]$

## Greek Symbols

Symbol	Description	Units
$\alpha$	Angle	$[degree]$
$\mu$	Dynamics viscosity	$[kgm^{-1}s^{-1}]$
$\Pi_{ij}$	Pressure-velocity gradient tensor	$[m^2s^{-3}]$

# Contents

<b>1</b>	<b>Introduction</b>	<b>1</b>
1.1	Background . . . . .	1
1.2	Flow description . . . . .	1
1.3	Thermal cooling . . . . .	2
1.4	Climate chambers . . . . .	4
1.5	Ultrasonic anemometer . . . . .	4
1.6	Similar works . . . . .	6
1.7	Aim . . . . .	7
1.8	Delimitations . . . . .	7
<b>2</b>	<b>Theory</b>	<b>9</b>
2.1	Turbulence . . . . .	9
2.2	Computational Fluid Dynamics . . . . .	10
2.2.1	CFD Overview . . . . .	11
2.2.2	Turbulence Modelling . . . . .	12
2.2.3	RANS methods . . . . .	14
2.2.4	Large Eddy Simulations (LES) . . . . .	15
2.2.5	Energy cascade and Turbulence spectrum . . . . .	15
2.2.6	Length and Time scales . . . . .	16
2.2.7	CFL condition . . . . .	17
2.2.8	Polyhedral mesh elements . . . . .	18
2.3	Heat transfer . . . . .	19
2.3.1	Conduction . . . . .	19
2.3.2	Convection . . . . .	20
2.3.3	Radiation . . . . .	21
2.3.4	Heat transfer in CFD . . . . .	22
<b>3</b>	<b>Method</b>	<b>24</b>
3.1	Experimental part . . . . .	24
3.1.1	Experimental apparatus . . . . .	24
3.1.2	Experimental setup . . . . .	25
3.1.3	Experimental trials . . . . .	26
3.2	CFD part . . . . .	28
3.2.1	Software used . . . . .	28
3.2.2	CFD domain . . . . .	28
3.2.3	Meshing . . . . .	30
3.2.4	Mesh Independence studies . . . . .	33
3.2.5	Boundary conditions . . . . .	34
3.2.6	Solver setup . . . . .	35
3.3	Post-processing procedure . . . . .	40
3.3.1	Averaging numerical data . . . . .	41
<b>4</b>	<b>Results</b>	<b>44</b>
4.1	Experimental results . . . . .	44
4.2	CFD simulation results and comparison . . . . .	48

<b>5 Discussion</b>	<b>57</b>
5.1 Numerical simulation setup . . . . .	57
5.2 Numerical results and validation . . . . .	57
5.3 Domain symmetry and non-symmetry consideration . . . . .	59
5.4 Flow behaviour inside the chamber . . . . .	60
<b>6 Conclusions</b>	<b>62</b>
<b>7 Future recommendations</b>	<b>63</b>

# 1 Introduction

## 1.1 Background

Reduction of turnaround time for the testing and developing new prototypes in the Research and Development (RD) sectors of a company is one of the prime aspects to cope up with competitiveness in the recent market scenario. Electronics cooling is one such aspect in the technical world, that has to do with the new designs and cooling techniques before getting it into production, for the equipment to deliver desired performance. Considerable amount of effort by thermal engineers needs to go into the cooling process of the electronic equipment, as the heat generated directly impacts the life span of equipment, reliability, operational safety and commercial competitiveness.

In the present internet dominant and dependent world, Telecommunication industries are the veteran and key players. Ericsson AB is one big giant in this sector. The role and service of these kind of industries is no more limited to merely connecting people at a distance by voice. They have vital contributions in the fields of automation, artificial intelligence, IoT (Internet of Things), data transport, cyber-physical systems, mobile edge computing, network security and the list goes on. There is a quest for more powerful, faster, accurate functionality from the electronic equipment, that these industries work on their day to day basis in order to keep the game on. Nowadays, there is an observable trend of the electronic gadgets of being portable, faster, compact and as a result of these getting hotter and hotter [1].

For each generation of electronic equipment there is a trend towards higher power densities and power dissipations, ensuing higher heat fluxes and larger temperature gradients, where the sophisticated need for the thermal cooling arises. Squeezing or integration of many components and the trend of reducing the size of the component than the previous model has posed challenge of dealing with non-uniform power dissipation. These are some undesired consequences of new designs and latest technology, that the thermal design unit in a company must handle. The goal of thermal design engineer/unit is to utilize the same volume to more efficiently transfer more heat from the equipment.

Though experimental techniques are believed to provide reliable and accurate results in the electronics cooling sector, the limited scope, expensiveness, and time factor are major concerns for the industrial business. Computational Fluid Dynamics (CFD), out of the various computational means and methods is a tool that keeps expanding its horizon, proving its versatile nature in application.[2] The advancements in the computing/computer technology has and is benefitting CFD to go for more detailed and meticulous simulations that are computational power hungry. CFD in the present days is widely used for numerical quantification and investigation of challenges involved in heat transfer and thermal cooling, considering the detailed level of results extracted from it.

## 1.2 Flow description

The flow in the chamber or outdoor conditions in general could be primarily categorised or characterised as laminar flow / turbulent flow, steady flow / unsteady flow, compressible / incompressible, viscous or inviscid and so on.[3] This may be due to the external

factors or the behaviour of the fluid itself under different circumstances and operating conditions. These kind of classifications provide an insight into the level of modelling and resolving that must be done in order to emulate the flow and provide close results. Here, the flow in the chamber is considered as turbulent and incompressible. As the flow involves natural convection, buoyancy-driven flow, the Rayleigh number characterises the flow to be laminar or to be turbulent. The variations in the density of the fluid as a result of heat transfer due to natural convection are minimal, considering the size of the test space volume and the heat source. Therefore, density variations can be neglected, which simplifies the solving of Navier-Stokes equation by the solver. However, the natural convection phenomena is still predominant here. The flow is unsteady here, considering the fact that air is forcefully introduced and removed from the test space volume (through inlet and outlet ducts). The air interacts with sharp corners of the radio unit, breaking down the laminar nature of the flow. Additionally, there is heat transfer from the radio unit which affects the flow characteristics of the fluid. Also, it is known that the turbulent flow is considered to be unsteady by its default nature. [3]

To build a baseline CFD model or a simulation it is helpful to understand the turbulence parameters that needs to be selected for the model. Turbulence parameters are defined in terms of Turbulent Kinetic energy, Turbulence Intensity, Length scales, Velocity scales, Eddy viscosity ratio, etc of the largest turbulent eddy structures present in the flow. As the flow comprises variety of eddy structure sizes, or a spectrum of different scales [4], a spectral analysis of the velocity variations with time can lead to the understanding of the operational range of the eddy structures in the flow. The outdoor data (velocity-time data) measured using in the site where the electronic equipment is put into use, is used for the spectral analysis. This gives a picture of the level of resolving that needs to be done in the numerical model, so as to capture the eddies in the fluid flow. The level of resolving needed determines the approach to be adopted (Either Laminar unsteady / Detached Eddy Simulations / Scale Adaptive Simulations / Unsteady Reynolds Averaging Navier-Stokes) to model the turbulence inside the climate chamber.

### 1.3 Thermal cooling

The goal of attaining improvised electronic equipment cooling can be achieved by exploring more complex and advanced heat sink geometries, optimizing the shape of fins and heat pipes, study the effectiveness using single fan or multiple fans or fan trays, assess the performance of thermal coatings and so on. Passive cooling is another area that is being constantly researched and explored. The companies, irrespective of their area of operation are constantly looking for and developing new metals or composites, thermal interface materials (TIM), phase change materials, fillers, polymers, greases, gels, thermal tapes, ceramics, semi-conductors that have better thermal properties than the traditional metals or alloys or compounds in use. The shape of the heat sinks or the vapor chambers is another area of focus, where there is enough research going on for the efficient shape required for taking out the heat generated by the equipment.

Traditional cooling theories and approaches widely practiced by the manufacturers are getting outdated (built-in thermal sensor technology, scaled down prototype testing and so on), thus failing to satisfy the present industry requirements. One of the current techniques of testing the electrical equipment includes testing in climate chambers, that emulate the outdoor atmospheric conditions for the equipment to be tested in. The cli-

mate chamber provides a space or volume for testing the electrical equipment that has natural convection like scenario as present in outdoor environments, by making use of centrifugal fans, blowers and heat exchanger units. Henceforth, the flow inside the climate chamber is a buoyancy driven flow, with slight variations in density due to the heat transfer involved from the testing equipment to the flow surrounding it. The flow is turbulent in most of the regions, transitional in less regions (in the cavities, between the fins of the heat sink) and has recirculation zones around the corners of the chamber.

These climate chambers employed for the purpose of thermal cooling tests, which have high capital investment, huge maintenance, less efficiency and offers limited results, leading to a compromise from the user side. This creates a need for an alternative promising method to replace the current system, that aids in saving unwanted usage of needy resources. A numerical model of the climate chamber can help solving most of the problems discussed above. Testing the electrical equipment virtually in a CFD model can give a better insight into the details of the heat transfer modes and mechanisms. Many new designs of heat sinks or vapor chambers or fan trays or integrated radio components, that are complex in terms of the structure or requires laborious and advanced techniques to manufacture the prototype can be virtually tested using CFD. And the merits and demerits can be qualitatively assessed with this CFD model of the climate chamber. The design space can therefore be enlarged for new designs. A virtual/CFD form of the climate chamber (CC) would empower the design process, while alleviating the usage of the climate chambers for such analyses. CFD offers a wide range of capabilities that lets the user change the operating and boundary conditions with great ease compared to that of the experimental setup. Boundary conditions here mean the various parameters that are involved in the heat transfer modelling like thermal resistance, heat flux, thermal conductivity, heat transfer coefficients, other similar constants and coefficients.

It is evident that everything comes at a cost. So does the CFD model of the virtual climate chamber. The disadvantages or the limitations of the CFD model are that, an exact replica or the flow with exact turbulent conditions as present in the outdoor environment cannot be modelled in the chamber. This comes from the fact of limited available resources in terms of computation and capturing data from the experimental apparatus for the desired level of details.

For the purpose of validation and providing initial data to build the numerical model, experiments are conducted in the climate chamber using the Ultrasonic anemometer, that captures the 3-dimensional velocities with a sampling frequency of 20[Hz]. On the experimental calculations side, there are constraints like, calibration of the equipment, accuracy of the data extracted from the equipment, means and methods of data extraction and processing, that can lead to possible errors in the data, diminishing the closeness of the results between the simulated and experimental results.

The measurements in this kind of climate chambers (CC) are mainly of outdoor products, whose cooling is based on natural convection. Forced cooling using fans is optional for these outdoor products. The CC in general provides only temperature measurement as the output to the analysis. The ability to visualize the flow characteristics is a valuable aid in the design process.

## 1.4 Climate chambers

Climate chambers or **Environmental chambers** are the closed circuit environments or more precisely huge enclosures, built for the purpose of carrying out tests on electronic equipment, industrial products, machinery, biological specimens and many other things[1]. These test specimens are tested for wide range of environmental conditions, to their working extreme conditions, by changing the operating conditions like velocity of air, temperature, humidity, vibration, soaking and so on. Some climate chambers are even capable of generating physical phenomena like corrosion onto the test specimen, by spraying salt or compounds that initiate corrosion.

These climate chambers allows for close monitoring of the performance and behaviour analysis by subjecting the specimen to desired operating conditions. Henceforth providing reliable results without the need for testing in the actual working sites, the research and design phase of products more economical in-terms of cost and time. Climate chambers comes in various sizes ranging from the size of small cooling refrigerator to the containers that can fit in a heavy duty truck.

Climate chamber functions are classified into three main categories:[1]

- Perform direct standalone variable environmental tests on the specimen
- Perform pre-processing or pre-analysis tests, which are followed by main course of tests
- Provide indirect means for testing specimen by providing suitable environmental conditions

The principle of operation of the climate chamber is that the changes in the operating parameters that govern the testing procedures. These alterations are achieved either by manual means, i.e, with direct manipulation in the integrated console or by remote access.

The climate chamber used in this thesis work is VCZ 50040-S from Vötsch, Industrietechnik. This is a walk-in chamber, with a test space volume of 36 m<sup>3</sup>, weighing 1300[Kg]. The climate chamber is equipped with a chiller machine for water cooling weighing about 1500[Kg]. It can provide an operating pressure ranging from 1 to 8 bars, compressed air consumption of 200 [m<sup>3</sup>/h], temperature range of -50 [°C] to +85 [°C] with a rate of 0.7 [K/min] of both heating and cooling. **Fig.1** shows the cross-sectional top view and the right view of the climate chamber. **Fig.2** shows the front view of the climate chamber, where the doors to the test volume space and the machine cabinet, where the console would be mounted is seen. The test volume space would be of the dimensions, 3600[mm] x 3000[mm] x 4030[mm], which includes a black box. The black-box mounted on to the back wall of the test space volume consists of 3 centrifugal fans close to the top, where the air is sucked in, heat exchangers in

## 1.5 Ultrasonic anemometer

Ultrasonic anemometers are the devices, that are used for measuring of accurate and reliable wind speed data along with the directions data. WindMaster 3-D Ultrasonic

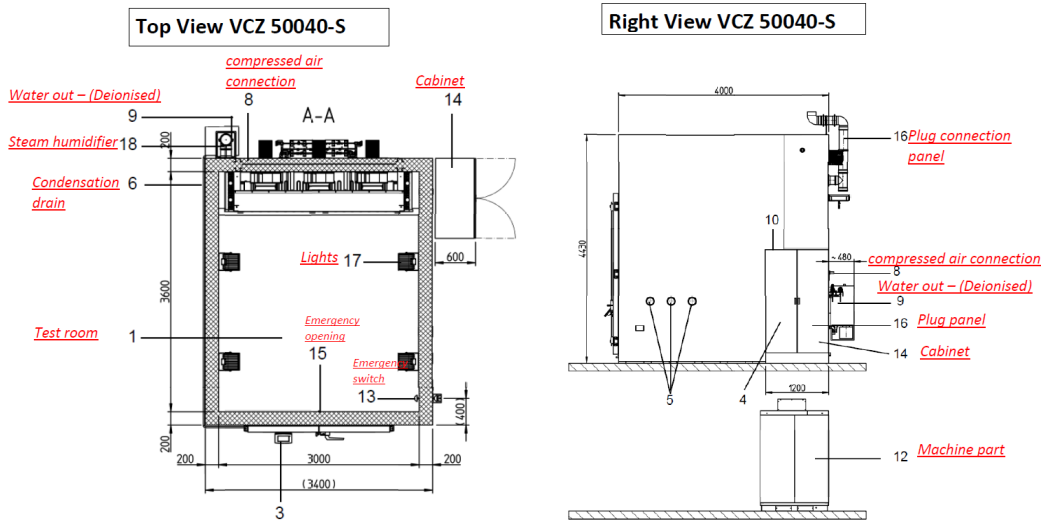


Figure 1: Top and Right view CAD drawings of the climate chamber

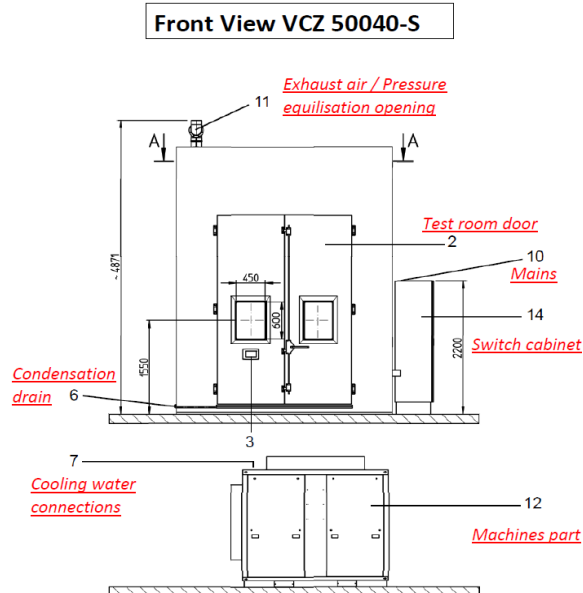
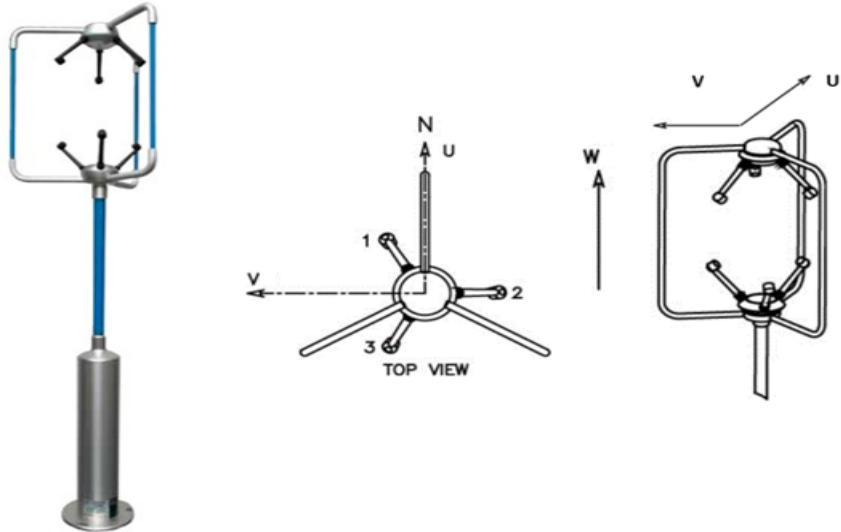


Figure 2: Front view CAD drawing of the climate chamber

Anemometer (by Gill Instruments) is used for carrying out experiments inside the climate chamber. The basic description of the anemometers used here is that, they are constructed in aluminum and carbon fiber and can perform wind velocity measurements in the three components of the velocity (longitudinal, lateral and vertical) of up to 45 [m/s]. These instruments operate with no moving mechanical parts, thereby going maintenance free. However, the sensors (transducers) in the anemometer are fragile and needs to be handled with care. The working principle of these anemometers is that, they use ultrasonic sound waves to measure wind velocity. Specifically, it measures the time taken for an ultrasonic pulse of sound to travel from an upper transducer to the opposite lower transducer, and compares it with another pulse from the lower transducer to the upper transducer. The sampling frequency of the anemometer used for the experiments

is 20 Hz.



**Figure 3: WindMaster 3D Ultrasonic Anemometer and U, V, W axis definitions from Gill instruments**

## 1.6 Similar works

Handful of works related to the thesis work, such as building a numerical modeling of a room or growth chambers [2], characterisation of indoor environments [3], numerical modeling of buoyancy-driven turbulent flows in enclosures [4], micro-level building thermal analysis [5], numerical study of turbulent mixing and laminar airflow for operating room ventilation [6], 3-D simulation of airflow and temperature variation in refrigeration cabinet [7], carried out in the field of CFD. However, particular projects similar to this master thesis work, involving modeling of heat transfer combined with spectral analysis were not found, as the other works are case specific, serving a different purpose.

The flow modelling in a growth/thermal chambers or modelling of an operation room to determine the effect of foreign bodies, follow the same initial steps as geometry creation and mesh generation, but use different techniques for solving based on the level of detail (particle tracking is involved which is not the case here) needed. One particular work [8], which is about the investigation of wind flow conditions provides a rough sketch of determining the turbulence by spectral analysis, present in the natural convection flows or outdoor flow.

A research work funded by NASA [9], has determined a procedure to calculate the length scales (both integral length scales and the dissipation scales) using the data acquired from the hot wire anemometry. In this journal, the experimental velocity data is processed into spectral data (power-spectral-density), thereby breaking down the complexity in understanding turbulence cascade . However, the paper relies on the Roach's equation (empirical formulae, explained in later sections) [10], which can be biased in comparison with other techniques (auto-correlation[11]) in estimating the integral length scales and the dissipation scales.

## **1.7 Aim**

The rationale of the present work is to fill the knowledge gap that is accumulated from the conventional testing procedures and the advanced testing procedures, by understanding to what extent a virtual climate chamber model can emulate a physical climate chamber or the outdoors, with reasonable resources. The aim of this master thesis project is to develop a numerical model of the physical walk-in climate chamber using commercial CFD software ANSYS Fluent.

The numerical model would emulate the outdoor environmental conditions closely, that are generated inside the physical climate chamber artificially. This model would then be used to carry out performance assessment test of the electronic equipment, when subjected to extreme climatic working conditions as done in the physical climate chamber. Heat transfer modeling and turbulence modeling of the flow inside the chamber is achieved using commercial CFD software, accounting for the flow unsteadiness and the structures present in the flow, as estimated by experimental means. The model is to be built with the inputs from the experiments conducted inside the climate chamber and validated with the same data. Identification the pros and cons of the developed model is aimed, thereby trying to go for a fail-safe numerical model of the chamber. The work flow algorithm of the thesis is presented in the **Fig.4**.

## **1.8 Delimitations**

- The time-span of the thesis work is limited to a period of 20 weeks, in order to meet the requirements of 30 ECTS
- Availability of the physical climate chamber to perform measurements and experiments are minimal due to on going priority projects in the company
- Level of detail in Turbulence modeling is mainly dependent on the availability of the computational resources provided by the company
- Complications involved when developing a numerical model, such as electromagnetic field effects, radio-frequency interactions, are neglected in order to implicate simplicity. In other words, Multiphysics modeling is not considered during numerical model build in the project.

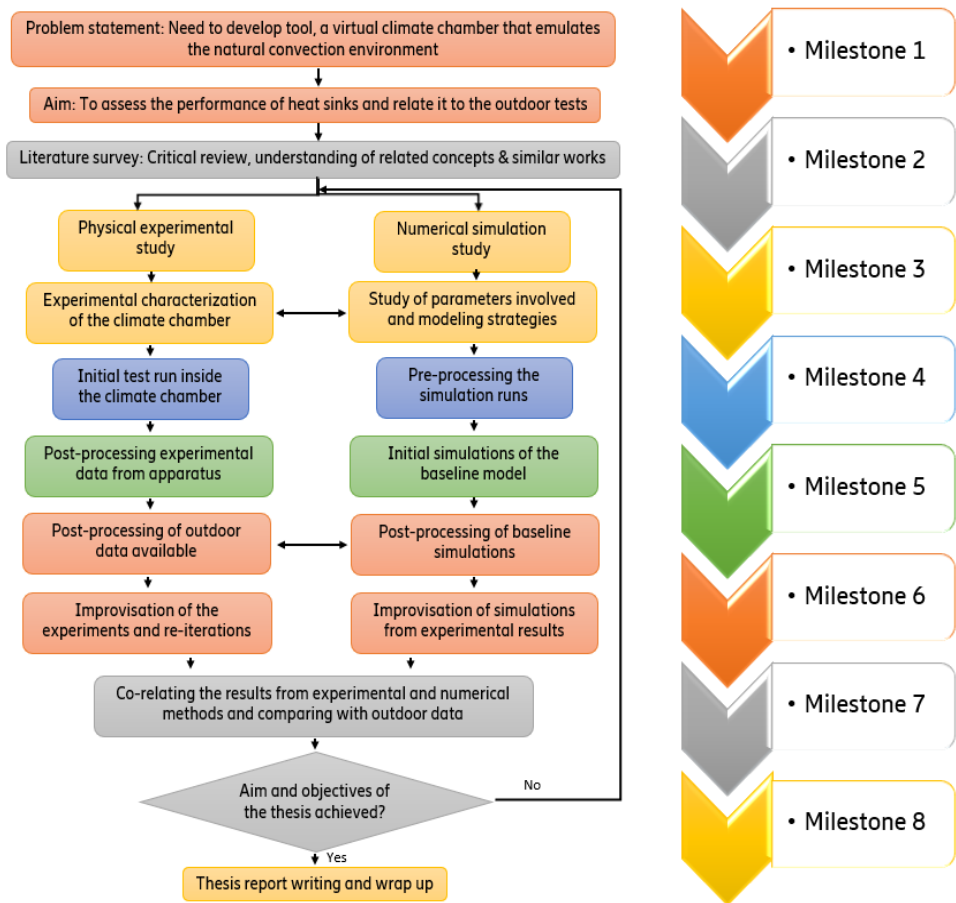


Figure 4: Thesis work flowchart, with all the tasks of the thesis structured into 8 milestones

## 2 Theory

### 2.1 Turbulence

As mentioned earlier a flow can be characterised into many categories based on the parameters of interest. Laminar flow and turbulent flow is one such categorisation. A dimensionless number, Reynolds number indicates if the flow is laminar or turbulent or in the transitional phase. This Reynolds number is expressed as the ratio of inertial forces to the viscous forces, **Eq.(1)** [12]

$$Re = \frac{\rho * V * L}{\mu} \quad (1)$$

The terms  $\rho$  and  $\mu$  are the fluid properties, density and dynamic viscosity respectively.  $V$  is the velocity scale, generally the average of the flow velocity and  $L$  is the length scale, which is typically the characteristic length over which the fluid flows (like radius of the pipe or the length of the plate in the generic examples used to explain the Reynolds number concept).

Laminar flow can be characterised as smooth flow, where the particles present in the flow are oriented in the direction of the flow, without any disorderliness. The flow is generally streamlined in nature, where there is no disruptions and lateral mixing happening among the adjacent layers. There isn't any formation of eddy structures or swirl flows or development of cross currents perpendicular to the direction of the flow.

Conversely, Turbulent flow is very hard to be put it into one single statement where all the traits of the flow can be expressed. There is no proper definition to define turbulence. Some of the major observable characteristics of a turbulent are listed below :

- Irregular and chaotic properties of the flow parameter, where the fluid motion is unsteady [13]
- Sudden variations of pressure and velocity of flow in space and time
- Presence of turbulent eddies that create fluctuations in velocity
- The vortices present in the fluid flow are of high intensities and high concentrations [14]
- Random and unpredictable nature of the flow
- Turbulent flows are by default three dimensional in nature[13], and have the rotationality trait
- Turbulence flows possess broad energy spectrum [15]
- Presence of energy cascade in the turbulent flow, where the larger eddies hand down the energies to smaller eddies and get further dissipated as heat energy
- Enhanced diffusion and dissipation in the fluid flows as a result of turbulent mixing
- Sensitive to the initial conditions, henceforth non-repeatable in nature [16]

- The length scales and the velocity scales of the structures found in the laminar flow are large and it is also noted that the smallest scales are sufficiently large enough to satisfy the continuum hypothesis [16]
- The turbulence can only occupy certain parts of the flow domain giving rise to intermittency [14]

Some of the pioneers in various fields have tried quoting the definition and understanding of turbulence in their own words. They are:

*"... the smallest eddies are almost numberless, and large things are rotated only by large eddies and not by small ones, and small things are turned by small eddies and large"*[16]

, a modern interpretation of the sketch that was found in a sketch book, which is believed that this book belongs to Da Vinci. This phenomena was termed as 'turbolenza' by Da Vinci, and thus was the birth of the term 'turbulence'.[16]

A description that closely explains turbulence, but still unclear in the sense of giving complete knowledge about turbulence is as follows:

*"Turbulence is any chaotic solution to the 3-D Navier-Stokes equations that is sensitive to initial data and which occurs as a result of successive instabilities of laminar flows as a bifurcation parameter is increased through a succession of values."*[17]

This description is more valid considering the facts that, it states that solution of the Navier-Stokes equations are associated with determining turbulence, which as of now is accepted by the modern fluid dynamics world. As in other definitions of turbulence, chaotic nature of turbulence is stated in the quote. 'Sensitivity to initial data' in the quote clearly speaks of the differentiation of irregular laminar flow from actual turbulent flow.[16]

## 2.2 Computational Fluid Dynamics

The numerical model is being developed using a branch of fluid mechanics, known as Computational Fluid Dynamics or CFD in short. By definition, CFD is a rapidly evolving science, that involves modeling, numerical analysis and data structures analysis to solve fluid flow problems using computational resources. Thus, proving meritorious to EFD (Experimental Fluid Dynamics) AFD (Analytical Fluid Dynamics)

CFD makes quantitative predictions of fluid-flow phenomena based on the governing laws or conservation laws of the fluid motion. By applying the fundamental laws of mechanics, the conservation of mass, momentum and energy are the ones that are on focus.[18] The governing equations include one continuity equation(2) as a result of conservation of mass.

$$\frac{\partial \rho}{\partial t} + \nabla \cdot (\rho V) = 0 \quad (2)$$

$$\frac{\partial \rho u}{\partial t} + \nabla \cdot (\rho u V) = -\frac{\partial p}{\partial x} + \frac{\partial \tau_{xx}}{\partial x} + \frac{\partial \tau_{yx}}{\partial y} + \frac{\partial \tau_{zx}}{\partial z} + \rho f_x \quad (3)$$

$$\frac{\partial \rho v}{\partial t} + \Delta \cdot (\rho v V) = -\frac{\partial p}{\partial y} + \frac{\partial \tau_{xy}}{\partial x} + \frac{\partial \tau_{yy}}{\partial y} + \frac{\partial \tau_{zy}}{\partial z} + \rho f_y \quad (4)$$

$$\frac{\partial \rho w}{\partial t} + \Delta \cdot (\rho w V) = -\frac{\partial p}{\partial z} + \frac{\partial \tau_{xz}}{\partial x} + \frac{\partial \tau_{yz}}{\partial y} + \frac{\partial \tau_{zz}}{\partial z} + \rho f_z \quad (5)$$

$$\begin{aligned} \frac{[\partial \rho(e + \frac{V^2}{2})]}{\partial t} + \Delta \cdot [\rho(e + \frac{V^2}{2}) V] &= \rho q + \frac{\partial}{\partial x}(k \frac{\partial T}{\partial x}) + \frac{\partial}{\partial y}(k \frac{\partial T}{\partial y}) + \frac{\partial}{\partial z}(k \frac{\partial T}{\partial z}) \\ &\quad - \frac{\partial(up)}{\partial x} - \frac{\partial(vp)}{\partial y} - \frac{\partial(wp)}{\partial z} \\ &\quad + \frac{\partial(u\tau_{xx})}{\partial x} + \frac{\partial(u\tau_{yx})}{\partial y} + \frac{\partial(u\tau_{zx})}{\partial z} \\ &\quad + \frac{\partial(v\tau_{xy})}{\partial x} + \frac{\partial(v\tau_{yy})}{\partial y} + \frac{\partial(v\tau_{zy})}{\partial z} \\ &\quad + \frac{\partial(w\tau_{xz})}{\partial x} + \frac{\partial(w\tau_{yz})}{\partial y} + \frac{\partial(w\tau_{zz})}{\partial z} + \rho f \cdot V \end{aligned} \quad (6)$$

Also, it has three momentum equations(3), (4), (5), for conservation of momentum, and one energy equation(6) for conservation of energy throughout the considered domain. These partial non-linear equations combined are collectively known as the Navier-Stokes equations. These set of five equations are solved simultaneously in an iterative manner in order to compute the flow parameters and fluid properties at any desired or all locations inside the considered area or volume of interest. The three momentum equations are similar but corresponds to three different spacial directions. In general, not all fluid flow problems can be solved practically using five basic governing equations. There are additional equations that are necessary, based on how the involved parameters are handled and the techniques used in solving. Some of these complex cases are, turbulence modeling, combustion, phase change of materials and so on.[19]

### 2.2.1 CFD Overview

In Computational Fluid Dynamics any given problem is broken down into three main interdependent sub-stages to get to the solution. They are:

- Pre-processing
- Solving
- Post-processing the obtained results

The pre-processing stage involves steps certain steps so as to foresee what needs to be expected from the CFD model. They include, Problem statement- where the goals, constraints, available resources are clearly evaluated and a plan is laid out. The physics that should be included, the operating conditions choice, the characteristics of the flow are carefully reviewed and decided. Geometry generation- A CAD (Computer Aided Design) model of the equipment or any other product on which the analysis needs to be carried out is built with or without implementing any necessary simplifications. Mesh/Grid

generation- the domain or the space of interest is broken down into numerous sub-domains, on which the governing equations would be applied and solved. This discretization of domain is a vital step in the pre-processing stage. Out of many discretization techniques the three important ones in context to the project are, FEM (Finite Element Method), FVM (Finite Volume Method) and FDM (Finite Difference Method). ANSYS Fluent software uses Finite Volume Method to discretize the grid, where the domain is divided into many smaller volumes. These smaller volumes are known as the mesh or grid elements.

In the Finite Volume Method approach, the governing equations are solved or represented and evaluated in the form of algebraic equations. These equations are generally solved for the flow parameters like pressure, velocity and temperature, at different nodes inside each cell of the discretized domains.[12]

In the second stage, processing and simulating of the problem is done. Onto the discretized volumes, the governing equations are solved in an iterative manner. The governing equations are solved in a coupled fashion simultaneously as a set/vector of equations or sequentially one after another. This is dependent on the choice of the solver made. The solver can be either pressure/density-based, coupled/segregated solver. Here a clear physical interpretation is made as the flux entering the considered volume is same as the flux leaving the volume. Henceforth, the discretized equations are applied and solved at each of the nodal points in the grid element[12]. Discretization schemes like central differencing, backward differencing, QUICK, Upwind schemes in space or time is adapted to calculate the fluxes and their gradients at the faces of the control volumes. There are approximations made when calculating these values at the nodal points, and the linearity of the equations play a defining role in choosing the schemes. The solutions, i.e, the set of the algebraic equations are then solved using a matrix solving procedure, preferably Gauss-Sidel technique in an iterative manner.[12].

In the final stage, the results obtained are qualitatively and quantitatively processed in order have a better representation of the physics in the problem visually and statistically. Various third party software are used in this stage to format and process the data. Verification and validation of the data from other techniques (AFD - Analytical Fluid Dynamics and EFD - Experimental Fluid Dynamics) are also compared in certain cases.

### **2.2.2 Turbulence Modelling**

Turbulence modeling procedure aims towards dissecting and understanding the physics underlying a turbulent flow, thereby predicting or capturing the average effects of turbulence with the help of Navier-Stokes equations. These solutions as said earlier, are either the averaged or mean properties of the flow parameters where the spatial/temporal resolution requirements are bounded/limited.[14] But this is not as simple as it sounds. As previously mentioned, turbulent flow is power packed with wide varieties of length and time scales, energy spectra, increased drags, huge dissipations, complex non-linear interactions, irregularities, irreversible stochastic phenomena and the list goes on.[14]

Solving the Navier-Stokes equations for a turbulent flow is quite challenging, considering the fact that equations are elliptic, non-linear and coupled (pressure-velocity, temperature-velocity)[20]. The flow consists of fluctuating velocity components and scales that have infinite degrees of freedom.[20] In order to model this turbulent flow successfully for the whole numerical resolution, a grid with number of nodes close to  $\text{Re}^{9/4}$  (at

the least, the number of cells in the grid vary as the Reynolds number is varied by this relation) is required.[20]. This fine grid resolves **all** the scales for a sufficient time interval, so that the properties of fluid attain a state of statistical equilibrium. Henceforth, Turbulence modeling is all about the manipulation of the governing and other related equations, thereby creating closed models (equal number of equations and equal number of unknowns), so as to simulate the turbulence generation and behaviour in the considered domain with known conditions.[14]

With the scope of the thesis in consideration, there are three main modeling frameworks that are interesting and useful to have better understanding. They are Reynolds-Averaged Navier-Stokes (RANS) equations, Large Eddy Simulations (LES) and Direct Numerical Simulations (DNS).

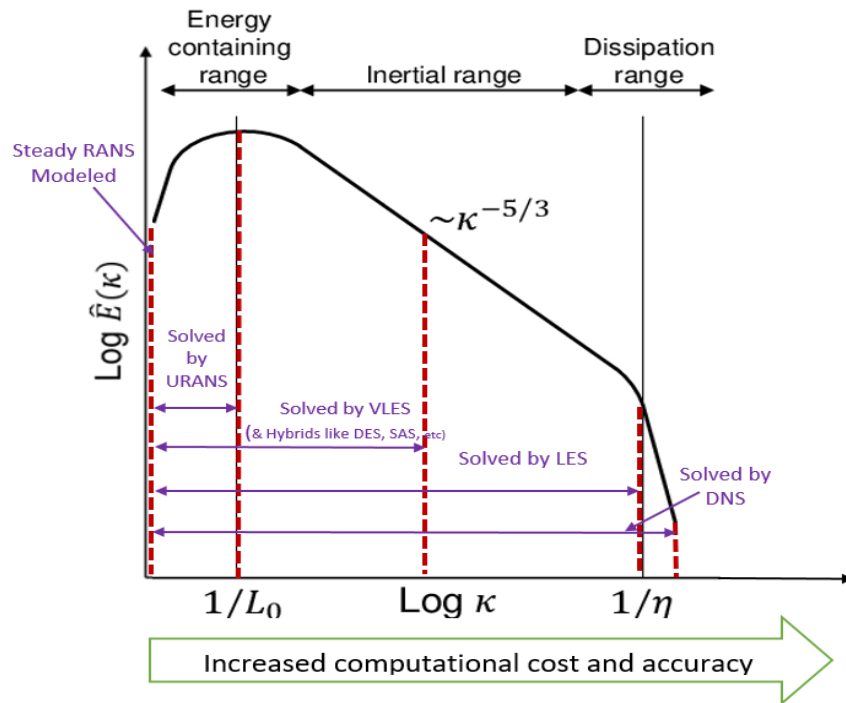


Figure 5: Level and extent of turbulence resolution or modeling capable by various strategies are shown, with the help of turbulence cascade graph. Logarithmic values Wave number on the abscissa and Turbulent Kinetic energy on the ordinate, with a slope of  $-5/3$  representing Kolmogorov's hypothesis of homogeneous, isotropic turbulence cascade [21] [22]

The graph in **Fig. 5**, [21] [22] represents the turbulence spectrum, which will be explained in detail in the upcoming sections. On the Y-axis is the Wavenumber and on the Y-axis is the Turbulence Spectral Energy. It can be seen that the URANS methodology resolves turbulence scales closer to  $1/L_0$  (Larger scales) and model the rest of the smaller scales. As we move towards the positive X-axis, it can be seen that the strategies tend to increase the level of resolution and decrease the modeling of the smaller dissipative scales. This increases the accuracy and computational resources needed. Eventually, DNS completely resolves all ranges of scales present in the flow, thereby not modelling any of the scales. This method requires insanely finer grid and lots of computational cores to run even run a smaller simulation.

### 2.2.3 RANS methods

In order to solve the Navier-Stokes equation with current day solving techniques, it is necessary to reduce number of scales (velocity scales), from infinity to a small number [20] This can be achieved by employing 'Reynolds averaging' or 'Reynolds decomposition' technique as depicted in **Fig. 6**. In this technique, random flow quantities/variables are decomposed or split into the mean component and fluctuating component. Reynolds decomposition is widely accepted from an engineering perspective, as the mean components are of prime importance rather than the turbulent or the fluctuating component [23]. However, with regard to the aim and scope of the thesis the turbulent part is more interesting and cannot be neglected. It is difficult to determine the exact solutions analytical or numerical methods,[21] there needs to be some kind of approximations made so as to obtain reliable solutions. In this RANS methods, complete dependency on the governing equations to understand the dynamics of the turbulence in the flow is avoided. Instead, assumptions are made about the behaviour of flow and incorporated into the turbulence models developed.[23]

Reynolds decomposition can be denoted as follows:

$$\Phi = \bar{\Phi} + \Phi' \quad (7)$$

Here,  $\Phi$  is the total component of a flow variable,  $\bar{\Phi}$  is the time-averaging or mean component and  $\Phi'$  is the fluctuating component

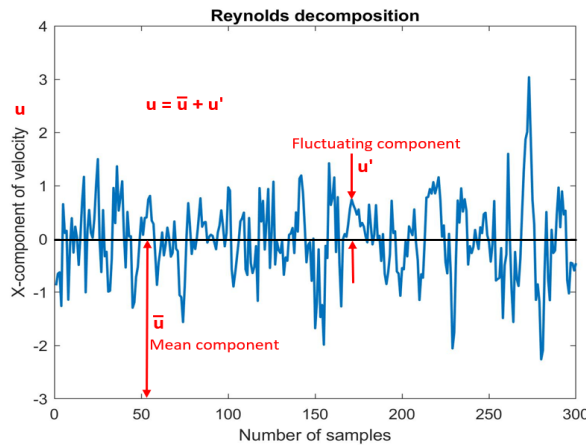


**Figure 6: Reynolds decomposition of velocity measured using ultrasound anemometer**

These mean and fluctuating components are substituted in the governing equations and further solved to obtain a processed set of equations. These equations represent or result in solutions that are exact for the averaged flow and not the turbulent part of the flow. From the definition of the Reynolds decomposition, the time average of the fluctuating components is taken to be zero, thereby reducing the number of terms in the final equations. [20] Instead, a new problem, termed as 'closure problem' arises due to the presence of unknown terms (turbulent stresses and turbulent fluxes). Henceforth, creating a mismatch between the number of unknowns and number of equations(for solving unknowns). Additional equations has to be introduced to solve for these unknowns, termed as 'Reynolds stresses'.

#### **2.2.4 Large Eddy Simulations (LES)**

Turbulent flow consists of turbulent eddies of various length scales and time scales. Large Eddy Simulations (LES) is one of the approaches used to resolve as well as model the unsteady turbulent flows. Complete resolution of eddies of all length and time scales are advantageous when solving a fluid flow problem. Direct Numerical Simulations resolve the entire spectra by numerically solving the Navier-Stokes equations using a fine mesh, without any need for modeling certain regions of the turbulence spectra. DNS requires super fine mesh cells to resolve the smallest dynamically significant scales (commonly known as the Kolmogorov scales) in the spectra, thereby spiking up the computational cost. In the current scenario, DNS is not a practical solution for most of the industry's day to day problems, considering cost that goes into diagnosing or research and development of a product. The level of detail provided by the DNS approach is also very high. Direct Numerical Simulations are time consuming and hectic for complex flow or geometry problems such as supersonic flows (high Reynolds number flows), turbulent jets, phase change materials, rotating frames, centrifugal pumps and so on.[12]

LES is a compromise between the RANS methods and the DNS method. The main goal of LES is to cut down the computational cost of simulations by having lesser mesh and resource requirements than DNS. In LES, the larger part of the turbulence spectra (length scales in the energy containing and inertial range) is resolved directly, and a turbulence model is employed to model the remaining part of the spectra (length scales in the dissipation range), as it is done in RANS method(however, LES involves spatial filtering and RANS involves temporal averaging techniques).[13] This is presented in the **Fig.5** Since the RANS model approaches solve only for the temporally averaged quantities, the effects of the instant turbulent motions is modeled using a turbulent model, it fails to predict transient phenomena and flow transition to acceptable limits [24]. LES model does not use time averaging or ensemble averaging of quantities along with the modeled equations to solve for the Reynolds stresses. LES method resolves the larger eddies that represent or contain the most of the turbulent kinetic energy of the flow. These eddies are responsible for vital phenomena like momentum transfer and turbulent mixing.[24]

#### **2.2.5 Energy cascade and Turbulence spectrum**

Energy cascade is one of the important and determining phenomena for the turbulence modeling. Commonly in Fluid Dynamics, an eddy structure is the identifiable structure in turbulence that spins.[25] These structures are created, when the boundary layer separation occurs and the flow being no longer attached to a certain surface . However, in certain cases when the fluid flows with a certain velocity over an obstacle, a region of vacuum is generated, triggering the oncoming fluid particles to undergo swirling motion at the edges of the obstacle, that are directed upstream to the back of the obstacle. Pope defined eddy as (Page 183, [11]) 'An eddy eludes precise definition, but is conceived to be a turbulent motion localized within a region of size  $l$ , that is at least moderately coherent over this region. The region occupied by a large eddy can also contain smaller eddies'. The size, in terms of length of these structures are referred to as the 'length scales' and the characteristic velocity of these scales are referred to as the 'velocity scales'. Turbulence length scales vary from the size of few millimeters to a few meters in length.

As put into words by Pope,(Page 182, [11]) 'Energy cascade is the process, where the kinetic energy of the fluid flow enters the integral length scales of motion(largest length

scales), as a result of the production mechanism in the flow'. The largest length scales are denoted as  $L_0$ . This kinetic energy is further transferred into smaller and much smaller scales by inviscid processes. This inviscid kinetic energy transfer occurs to the smallest scales, till the energy is finally dissipated into heat by the viscous action of the fluid particles. The dissipation phenomenon is denoted by  $\epsilon$ , which is energy per unit time and unit mass [ $\text{m}^2/\text{s}^3$ ].

Smallest scales are known as the dissipative scales which were identified by Kolmogorov, hence giving the name Kolmogorov scales. These scales are denoted by  $\eta$ . Kolmogorov scales are independent of the Reynolds number of the flow, where as the integral scales are dependent on the Reynolds number. At these smallest scales viscous forces dominates over the inertial forces (the frictional forces in the smallest scales are largest compared to other scales), thereby transforming the kinetic energy into thermal energy. Henceforth, the size of the Kolmogorov scales are determined by the viscosity,  $\nu$ .

## 2.2.6 Length and Time scales

The variations in the length and time scales, (between the integral and Kolmogorov scales) is an important characteristic feature of any given turbulent flow. However, it is this variations that is responsible for the numerical and experimental analysis of the flows. Primary concern that one has to look for when discussing about the turbulent flows / turbulence modeling is, to closely distinguish between small-scale motions and the large scale motions in turbulent flows.[26] Determining the length and time scales of the characteristic scales, i.e, the largest scales in the considered domain is of prime importance when building a numerical or an experimental model. A general assumption is made that around 90% of energy in the turbulence spectra goes into the larger scales. [27] There are wide range of scales that are present in a turbulent flow. Knowledge about the energy transfer phenomena, such as production and dissipation is also a requirement for efficient turbulence modeling.

In the current thesis work, physical constraints, i.e, the capability of the ultrasonic anemometer (the maximum possible frequency at which the data is captured) is a determining factor for the range of lengths of the turbulent eddy scales inside the turbulence spectrum. Length scales indicate the size of the rotational structures in the flow, they are a key asset in computational analysis as the longest ones serve to delimit the size of the elements in the medium.

An integral length scale represents an average of all turbulent scales in present in the flow. The magnitudes of the integral length larger scales are dependent on the larger eddies in the flow, that contain most of the energy in the spectrum. Generally, the larger scales in the spectra are of the order of flow geometry (boundary layer thickness), having length scale  $L_0$  and velocity scale  $U$ . The eddies with integral length scales extract the kinetic energy from the mean flow, as the mean flow has time scales that are comparable to the larger scales.[27] Larger eddies are more random in nature, anisotropic, and their behaviours is affected by the body forces, geometry, boundary conditions and the operating conditions. Whereas the smaller eddies are modeled with an assumption of being isotropic in nature. Henceforth, the larger eddies or the eddies of integral length scales have greater impact on the nature of the flow and these need to be resolved.[2]

From Kolmogorov's first similarity hypothesis, 'In every turbulent flow, at sufficiently high Reynolds number, the statistics of the small scale motions have a universal form

and are uniquely determined by overall kinetic energy production rate (i.e, the dissipation rate,  $\epsilon$ ) and viscosity  $\nu$  [27]. The dissipation rate will be independent of viscosity, however the scales at which the kinetic energy is dissipated will be dependent on both dissipation rate and viscosity. The Kolmogorov length scales can be estimated from formula (8), time scale from formula (9) and velocity scales from formula (10). [23]

$$\eta = \left( \frac{\nu^3}{\epsilon} \right)^{\left(\frac{1}{4}\right)} \quad (8)$$

$$t_\eta = \left( \frac{\nu}{\epsilon} \right)^{\left(\frac{1}{2}\right)} \quad (9)$$

$$u = \left( \nu \epsilon \right)^{\left(\frac{1}{4}\right)} \quad (10)$$

In order to relate the Kolmogorov length scales to the integral length scales, the dissipation rate of Kolmogorov scales must be expressed in terms of the large scale flow characteristics. An approximation is made that the kinetic energy of the flow is proportional to  $U^2$  and the time scale as  $L_0/U$ . Substituting these approximations for dissipation rate  $\epsilon$ , we obtain the relation between Integral and Kolmogorov length scales (11), and time scales (12).

$$\eta = \left( \frac{\nu^3 L_0}{U^3} \right)^{\left(\frac{1}{4}\right)} \quad (11)$$

$$t_\eta = \left( \frac{\nu L_0}{U^3} \right) \quad (12)$$

The graph in Fig.(7) represents the spectrum for the energy. It is the variation of the energy with respect to the wave numbers,  $k$ . Wave number is inversely proportional to the eddy size,  $k$ .

Fig. 6 illustrates schematically the variation of energy content with wave number, which is inversely proportional to the eddy size  $l$  according to The abscissa could also have shown frequency associated with the eddies, as this varies similarly to the wave number

### 2.2.7 CFL condition

The Courant - Friedrich's - Lewy condition is used to gain stability or stabilize unstable numerical methods, that model convection or wave phenomena. This condition states that the distance travelled by the information within the mesh cells, at one time step length must be lesser than the distance between two consecutive mesh elements. If the time-step length is larger then there might be instability in the nature of results, affecting the convergence. [28]

The final formula for Courant number, a dimensionless quantity, is expressed as formula,(13)

$$C = a \frac{\Delta t}{\Delta x} \quad (13)$$

The Courant number value must be lesser than or equal to 1, so as to avoid passing of information to more than one cell at one time step.[28]. Lesser courant number aids in

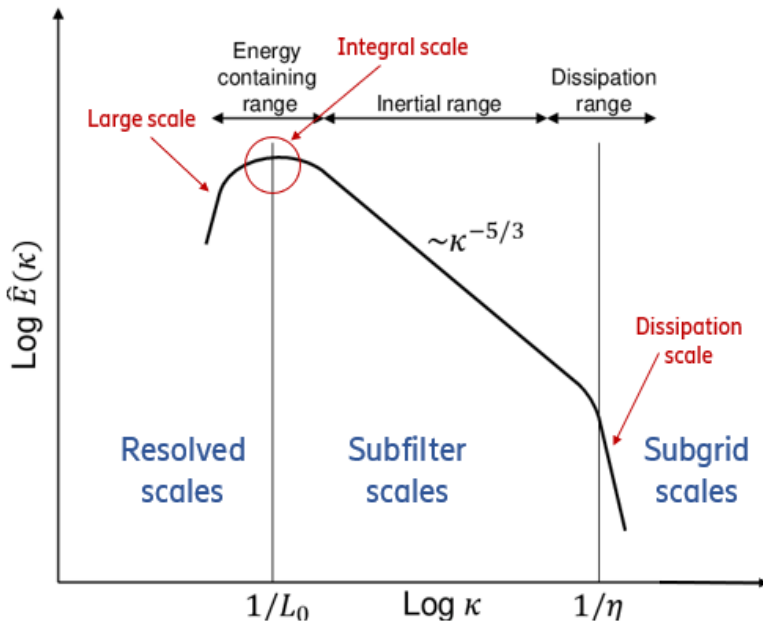


**Figure 7: Length scales in the turbulence spectra, showing various orders of length scales. Integral length scales are the largest length scales, containing most of the energy present in the spectrum. In the dissipation range, the length scales are known as the Taylor's scale and Kolmogorov's scales that need extremely fine mesh in order to be resolved**

achieving the convergence of the residuals. The Courant number can be reduced using two methods in the current work (transient simulations). They are:

- Lower time step value in a transient simulation (steady state simulations are of not much importance here)
- Reduce the fineness of the mesh in the critical areas, making them coarser (however, coarser mesh is incapable of resolving the scales to a detailed extent as a finer mesh would facilitate)

### 2.2.8 Polyhedral mesh elements

Polyhedral mesh elements are used in the mesh generation. This choice of the type of the mesh element comes from the advantages that the Polyhedral mesh has over the tetrahedral and hexahedral mesh elements. Polyhedral mesh, as the name indicates has many faces compared to the tetrahedral mesh elements, making the faces contact with many adjacent cells. This leads in better approximation of the flux gradients and have higher numerical stabilities.[29] A polyhedral mesh element corresponds to a smaller chunk of the three dimensional domain. This type of partition proposed by physicist Denis Weaire and Robert Phelan, and it is 0.3% more efficient than a complete 14 sided, tetrakaidekahedron cells arrangement, proposed by Lord Kelvin in 1887 [30].

Tetrahedral elements cannot be effectively stretched without decreasing the overall mesh quality factor.[31] Polyhedral mesh elements are less sensitive to stretching of mesh elements when compared to tetrahedral elements, providing increased numerical stability of the numerical model as the numerical diffusion is low. (Polyhedral elements

have mass exchange over many faces compared to tetrahedrons).[31] Also, the mesh cell count a geometry when using polyhedral elements compared to tetrahedral elements is much lower.

## 2.3 Heat transfer

Heat transfer is a discipline in thermal engineering that deals about the flow of energy (heat energy transfer) between different bodies due to the temperature gradients. The material bodies can either be solids or fluids or in transitional states. Temperature and heat are two things which are mistaken to be same things, but they are very distinct. Temperature can be defined as the degree of hotness, which is a measure of a quantity. Whereas, heat is a form of energy that is in transit.[32] Heat transfer provides information about, the mode of transfer of energy, the rate ( $dQ$ ) at which the energy is transferred and also some details about the temperature distribution inside the body.[32] Heat transfer is governed by law of conservation of energy (first law of thermodynamics) and second law of thermodynamics.

The heat energy flows from any physical entity to the surroundings in which it is present whenever there is temperature difference. It can happen in a natural (buoyancy driven flows) or forced (external fans, radiators) manner, if the mode of heat transfer is convection. If at all the body is perfectly insulated, so that the heat transfer does not occur through the walls of the body, then the body is considered to be adiabatic in nature. The heat transfer also cannot take place once the thermal equilibrium is reached, where the bodies are isothermal (of same temperature).

Heat transfer occurs in three different modes. They are thermal conduction, thermal convection and thermal radiation. These are classified based on the mediums through which the heat exchange takes place. There are other means of heat transfer namely advection and heat transfer through phase changes, which are not of much importance here.[32]

### 2.3.1 Conduction

In conduction the flow of heat occurs through the solids and liquids by vibration and collision of molecules and free electrons present within the solids or liquids. The heat energy flows from the high temperature body to the low temperature body, when the solid bodies are in contact. In certain cases, if the different components of a same parent body are in contact, then heat transfer can occur through conduction. At the microscopic levels, it can be explained as the vibration of atoms (at that part of solid body, where heat is supplied) lead to collision with the neighbouring atoms thereby transferring heat energy. The motion or vibration is only in the molecular level and the body as a whole has no motion. **Eq.(14)**.The rate of heat transfer is directly proportional to the normal temperature gradient.[33] The law of heat conduction, Fourier's first law of thermodynamics explains the conduction mechanism or conductivity, which is **Eq.(14)**.

$$q_x = -kA \frac{\partial T}{\partial x} \quad (14)$$

Here,  $k$  is the proportionality constant or the conduction coefficient [W/mK],  $q_x$  is the rate of heat transfer [W], and  $\frac{\partial T}{\partial x}$  is the temperature gradient in the direction of heat

transfer [K/m]. In conduction mechanism the heat transfer is dependent on the material properties, area of the cross-section, temperature gradients and the path length of the heat transfer. Henceforth, thermal conductivity  $k$ , is a material property, which varies accordingly with the temperature of the material. The general three dimensional equation for heat transfer can be written as,

$$\frac{\partial}{\partial x}(k \frac{\partial T}{\partial x}) + \frac{\partial}{\partial y}(k \frac{\partial T}{\partial y}) + \frac{\partial}{\partial z}(k \frac{\partial T}{\partial z}) + \dot{q} = \rho c_p \frac{\partial T}{\partial t} \quad (15)$$

where,  $\rho$  is the density of the material [Kg/m<sup>3</sup>],  $\dot{q}$  is the rate of heat transfer per unit volume [W/m<sup>3</sup>] and  $c_p$  is the specific heat of the material [J/Kg.K] This equation considers the heat transfer in all three coordinate directions. On considering constant thermal conductivity, a new parameter is introduced into the Eq.(15), called thermal diffusivity  $\alpha = k/\rho c_p$ . The higher the thermal diffusivity of a material, higher is the rate of transfer through it.[33]

### 2.3.2 Convection

Thermal convection is the heat transfer carried out by the mass motion of the fluid (liquids or gases) when the heat is supplied through a heat source. Usually convection takes place due to density variation which in turn is a result of temperature gradients. The heat convected away depends on the temperature gradient and the characteristics of the fluid (laminar or turbulent). Convection occurs when the fluid around the heated surface gets less denser moves away making space for the cooler fluid which is more denser in nature. However, it is evident that the heat transfer mechanism at the wall (of a solid body) is always conduction process,[33] Newton's law of cooling Eq.(16) explains the mechanism of convection. The law of cooling by Newton states that, 'the rate of heat loss in a body is proportional to the difference in temperatures between the body and its surroundings, while under the effect of a breeze'.[33]

$$q = hA(T_w - T_\infty) \quad (16)$$

In the above equation,  $h$  is the proportionality constant, i.e, heat transfer coefficient [W/m<sup>2</sup>K],  $T_w$  is the wall temperature,  $T_\infty$  is the freestream temperature of the fluid,  $A$  is the surface area and  $q$  is the rate of heat transfer [W]. The heat transfer coefficient is assumed to be constant for many simpler analysis, but in reality it varies accordingly with the flow temperature and flow characteristics, flow velocity and so on, making the analysis more complex. The heat-transfer coefficient can also be sometimes called the 'film conductance', due to the fact that the heat transfer right next to the wall is considered to be conduction mechanism with the the thin stationary layer of fluid at the wall surface.[33] Heat Transfer Coefficient depends on the flow and also it represents the thermal resistance of the steady layer of fluid particles present between the heat source wall and the fluid medium. Thermal resistance is a material property, which defines the quantity of resistance offered by the material itself to the heat flow across it. Convection can be classified into two major categories based on the influence of the external factors on to the velocity of the fluid surrounding the body. They are free or natural convection and forced convection.

Natural convection or the free convection phenomena occurs when the heat transfer and the bulk fluid motion around the body is caused by buoyancy forces. These natural

buoyancy forces that result from the density variations caused by the temperature gradients between the heat source and the fluid surrounding it. The fluid in the close vicinity of the heat source gets less denser, as the molecules start vibrating and are excited, leading to the separation and scattering phenomena. In other words this process can be termed as thermal expansion. The more denser fluid around this lesser denser fluid displaces and the process repeats. Along with the displacement of the fluid the heat energy is also transported or convected away. Thus the heat transfer takes place from the hotter volume to the cooler volume of the fluid under the influence of buoyant forces.[34]. For natural convection mechanisms the heat transfer coefficient,  $h$  varies between 0.5-4000 [W/m<sup>2</sup>K] (The lower values correspond).[35] Since the fluid velocity associated in natural convection is dependent on the natural forces, the velocity is low, leading to lesser heat transfer rates and less heat transfer coefficients. Natural convection can occur only in the presence of acceleration due to gravity or similar other forces like the Coriolis force or centrifugal force.[36]

Forced convection is the other type of convection where the fluids surrounding the heat source are forced to move using external factors, increasing the flow velocities which in turn amplifies the rate of heat transfer. The external factors are centrifugal fans, pumps, ceiling fans, exhaust fans, suction and so on, that stir and steer the air enhancing the heat transfer. Forced convection can also be expressed by the Newton's law of heating and cooling.

It is important to note that, when the velocity of the fluid surrounding the body is zero, then the heat transfer mechanism would occur only through conduction mechanism. Natural convection is the predominant phenomena within the scope of this thesis work. The performance of the radio units and the heat sinks that are developed are tested in the environments where natural convection scenario can be reproduced using artificial means (here the climate chamber). Though there are centrifugal fans present in the physical climate chamber, the heat energy transfer mechanism cannot be considered as the forced convection. This comes from the fact that the wind or air velocities inside the climate chamber are as low as experienced in the outdoor scenarios. The effects of the buoyancy forces are successfully achieved inside the climate chamber and the effects of humidity are neglected for the purpose of simplification.

### 2.3.3 Radiation

Radiation is the mechanism that does not require any material medium for heat energy transfer from a hotter body to a colder body. Both conduction and convection mechanisms require solids or fluid medium, whereas radiation can achieve even in perfect vacuum conditions. The heat is propagated in terms of electromagnetic rays, that are also known as thermal radiation.[33]

The thermal radiation phenomena is quite complex in nature and it can be expressed in simple terms using Stefan-Boltzmann law. The Stefan-Boltzmann law states that the radiation energy per unit time from a black body is directly proportional to the fourth power of absolute temperature. It is expressed as Eq.(17),

$$q = \epsilon\sigma A(T_1^4 - T_2^4) \quad (17)$$

In Eq.(17),  $q$  is the rate of heat transfer [W].  $\epsilon$  is the emissivity of the surfaces radiating,  $\sigma = 5.669 \times 10^{-8}$  is Stefan-Boltzmann constant [W/m<sup>2</sup>K<sup>4</sup>],  $T_1$  and  $T_2$  are the surface

temperatures [K] and  $A$  is the surface area [ $\text{m}^2$ ].

Considering the fact that all materials that have temperature above zero [K] (Absolute zero temperature), are capable of emitting thermal radiations, heat sinks radiate certain percentage of total heat dissipated from the surfaces.[37] The heat sinks contains many surfaces that are exposed to the outer surroundings where considerable amount of heat is radiated. The measure of amount of heat dissipated through radiation is vital when analysing the performance of the heat sinks. Comparing to the quantity of heat dissipated through convection, radiation accounts for a very little part (conclusion from the previous studies conducted on the electronic equipment in the company), which is taken into consideration when building the numerical model.

### 2.3.4 Heat transfer in CFD

Heat transfer modeling is meritorious compared to experimental and analytical calculations of heat transfer in many ways. As discussed earlier a CFD model provides greater detailed insight into the multiple underlying phenomena in heat transfer and turbulence modeling. ANSYS Fluent solves heat transfer problems by combination of energy equation and the flow equations. Energy equation is primarily responsible for the heat transfer modeling in a fluid dynamics problem. Conjugate heat transfer technique or methodology in CFD refers to the ability of the CFD solver to compute heat transfer by conduction in solids, which are coupled with heat transfer through convection in fluids.[35] Numerical model of the climate chamber would include heat transfers in both conduction and natural convection forms, developing a need for conjugate heat transfer modeling.

In case of incompressible fluids, i,e, fluid flows having low velocities, pressure based solvers are preferred. These pressure based solvers consider that the variation in density is very negligible (or almost assume constant density), therefore decoupling the energy equation and the mass conservation combined with momentum conservation equations. In such cases the energy equations can be exempted from the calculations when solving for the flow field parameters. However, as the heat transfer modeling is made, the energy equation is solved with the mass and momentum conservation equations to solve the temperature field. [12]

Many phenomena in heat transfer like viscous dissipation, species dissipation, inter-phase energy source (phase change) can be modeled in CFD. ANSYS Fluent solver solves the energy equation in this form of transport equation, **Eq.(18)** cited from [38].

$$\underbrace{\frac{\partial(\rho E)}{\partial t}}_{\text{Unsteady}} + \underbrace{\nabla \cdot [V(\rho E + P)]}_{\text{Convection}} = \nabla \cdot \left\{ \underbrace{k_{eff} \nabla T}_{\text{Conduction}} - \underbrace{\sum_j h_j J_j}_{\text{Species diffusion}} + \underbrace{(\overline{\tau_{eff}} \cdot \vec{V})}_{\text{Viscous dissipation}} + S_h \right\} \quad (18)$$

In case of only solid components (only conduction mechanism) in the flow problem, the fluid transport equations need not be solved, but energy equation must be solved to solved to obtain the temperature values in the considered domain. In the **Eq.(18)**  $E$  is the energy per unit mass.  $k_{eff}$  is the effective conductivity ( $k + k_t$ ), where ( $k_t$ ) is the turbulent thermal conductivity that is defined according to the turbulence model used.(However, there is no turbulence model employed in the current thesis work) The energy sources due to viscous dissipation and species diffusion play an important role if the flows are

compressible in nature.[38] As the flow inside the climate chamber is considered to be incompressible, these terms are neglected.  $S_h$  is the Enthalpy source or sink term. This source term includes the effects of heat transfer due to radiation. The thermal boundary conditions can be specified in the Fluent solver in five different types. They are heat flux, temperature, convection, radiation and mixed boundary conditions.[38] For solid materials, wall thickness or shell thickness, heat generation rate per unit volume can be defined. Coupled thermal boundary conditions are available in Fluent solver so that conjugate heat transfer modeling can be achieved.

Boussinesq hypothesis approximation is implemented to specify the density of the fluid inside the climate chamber in the numerical model. The Boussinesq model considers the density of the fluid to be uniform in all the governing equations, except for the body forces term in the momentum equation along the direction of gravity. This simplification reduces the complexity of solving the governing equations by a large extent. In natural convection problems, using the Boussinesq approximation leads to faster convergence and reduces the non-linear nature.[38] However, this can be considered only when the density variations are too small.

# 3 Method

In this chapter of the report, the methodology that was implemented during the thesis work will be explained. Initially, a brief explanation of the experimental part will be done. Later on the major focus of this thesis work, computational methods and details involved in the building of the numerical climate chamber model will be put out extensively.

## 3.1 Experimental part

### 3.1.1 Experimental apparatus

A radio unit, with two heat pads stuck on to an aluminium enclosure, and conventional fins was used to carry out the experiments. This unit, provided by Ericsson AB, will serve as heat source, so to compare how the temperature dissipates as wind speed increases. The radio has vertical fins on one of the face only, which is the heat sink, dissipating heat to the surroundings. There are two heat pads, green coloured mats, (as shown in **Fig. 8**) mounted on to the inner walls of the radio unit, vertically one below the other, that act as the actual heat generating sources. The upper heat pad, which is numbered 1 (white coloured font), produces a nominal heat power output of 150 watts and the lower one, numbered 2, produces about 50 watts when plugged into power supply unit (PSU). The power given to each mat can independently be controlled using both channels in PSU.

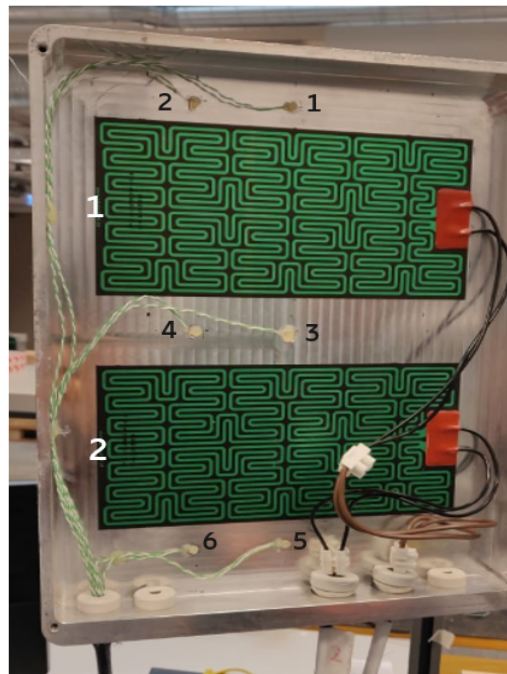


**Figure 8:** Cross-section of the radio unit with thermocouples. The green mats are the heating pads responsible for the generation of heat, and generate about  $7500[\text{kW}/\text{m}^3]$  (Upper heat pad) and  $2500[\text{kW}/\text{m}^3]$  (Lower heat pad)

**K-type thermocouples** are used as probes to get the temperature around the heat pads, that are stuck to the inner core of the radio unit. The k-type thermocouples log temperature readings in a temperature range between 20°C and 70°C. Six thermocouples are glued to specific points on the inner side of the aluminium enclosure, around the heat pads (marked from 1 to 6 black font in the picture). The thermocouple cables are connected to a data logger that logs the temperature readings every one second.

Other apparatus used in for carrying out experiments include,

- **Converter**- which converts analog signals from the anemometer to digital signals, which will be further processed using the software (provided by Anemometer's manufacturer)
- **Data logger**- This device functions similarly to the converter, that converts the thermocouple readings into temperature data that is readable by the computer
- **Power Supply Unit (PSU)**- facilitates to vary the voltage and current that is being supplied to the mock-up radio unit by tuning to the desired values, so as to control the heating of the radio unit

### 3.1.2 Experimental setup

Main goal of conducting experiments is to log the fluid flow (air) velocity inside the climate chamber using the ultrasonic anemometer and record temperature data from the thermocouples placed in and around the radio unit. This is done for varying fan speeds (outlet duct centrifugal fan speeds), which alters the average flow speed of air over the radio unit, that is put out for testing at ambient room temperature of 25[°C]. The humidity levels inside the chamber are set to zero, complying with the standard test procedures used by the company in earlier tests, thereby reducing one parameter governing the flow. However, there is humidity factor present in an actual natural convection scenario.

The fan speed settings, 30%, 50% and 100% are preferred, in order to match the previous thermal tests conducted by the company in the same climate chamber. By fan speed settings, it means the velocity of the exhaust centrifugal fans that are located close to the roof of the climate chamber. When the velocity of rotation of the fans increase, a larger volume of air is being sucked into them, thereby increasing the volume of the air that is forced into the chamber. The velocity of the air being forced into the test space volume at the inlet would range from 0.8-2.5 [m/s] for the chosen fan speed settings.

In order to characterize the test environment, i.e, test space volume inside physical walk in climate chamber, four fixed locations are selected, which are at same distance, away from the radio unit. The radio unit is placed at the centre in the control volume, at a height of 1.5 [m] from the ground level. The position of anemometers are depicted using numbering 1, 2, 3 and 4 as shown in the **Fig. 9**, and the position of radio unit is indicated by the blue cross mark.

As mentioned earlier, the apparatus used to measure wind speed values inside the climate chamber, are two ultrasonic anemometers developed by Gill Instruments. These ultrasonic anemometers are set to log data at a sampling frequency of 20[Hz]. These

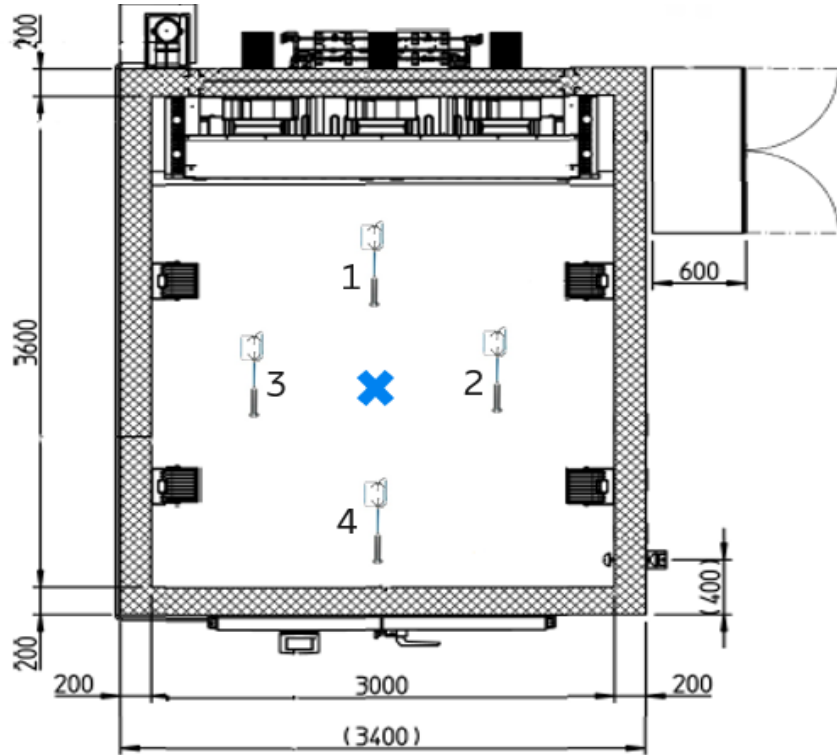


**Figure 9: Top-view of the CC, presenting the position of four anemometers in the test space volume with the radio unit in the centre indicated by blue cross mark**

anemometers record lateral, longitudinal and vertical components of velocity. Longitudinal and lateral components configure the (x,y) plane, while the vertical component represents the perpendicular axis to the (x,y) plane.

### 3.1.3 Experimental trials

The experimental test apparatus were arranged as shown in the schematic representation in **Fig. 10** and the physical arrangement as shown in **Fig. 11**. The openings in the climate chamber, for wires and hoses were completely sealed so that there is no leakage of air, thereby making it a closed system where there is no heat transfer to the outer surroundings. The walls of the climate chamber are considered to be insulated, even though they conduct negligible amounts of heat.

The power is supplied from the PSU to the radio unit, without switching on the chamber. The radio unit heats up to its full power, till the surface temperature of the radio unit is stabilized. The temperature in the climate chamber is set to ambient temperature of about 25[°C] and eventually 30%, 50% and 100% fan speeds are tested. The average velocity of air at the inlet varies from 0.5 [m/s] to 2.5 [m/s], on varying the fan speeds.

The velocities of air in all three directions (x, y and z components) is measured using ultrasonic anemometers, placed at the specified positions and the data is logged using data logger. Similarly, the probe temperatures are measured using the thermocouples placed around the heat pads and the whole radio unit.

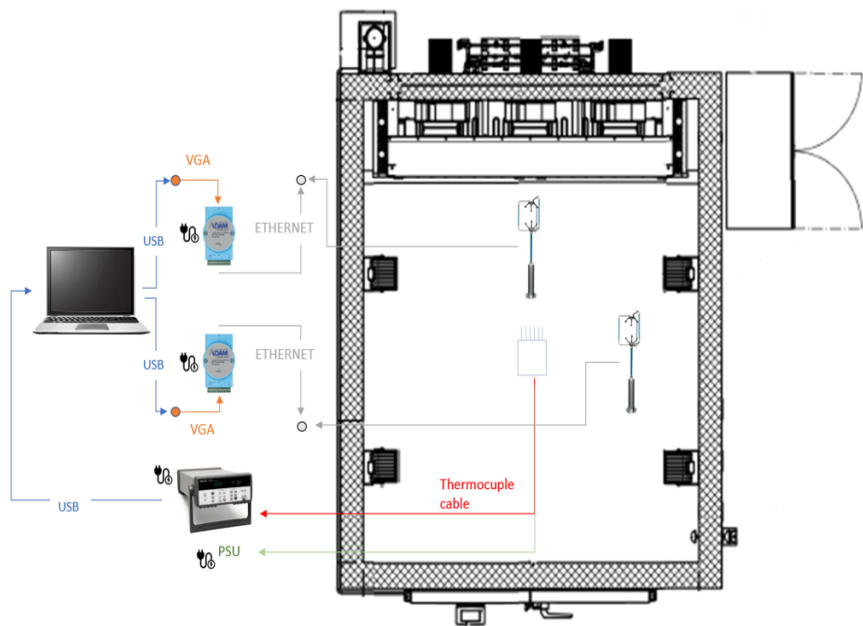


**Figure 10: Experimental test apparatus arrangement including Radio unit, anemometers, power supply unit, data loggers and connection cables**



**Figure 11: Front-view of the CC, presenting two anemometers and the radio unit mounted on to the stand, with temperature probes attached to the radio unit. The wires lying on the floor, were tied up at the height of the anemometer mounting stands during the experiments. This is done, so that air would have a clear path as much as possible as depicted in geometric model in further sections**

## 3.2 CFD part

A numerical model is a representation of an actual working physical system, where this physical system is described using the numerical concepts. The purpose of building a numerical model is mainly to understand the behaviour and explain the same, when certain functionalities are changed, resulting in different configurations.

### 3.2.1 Software used

ANSYS Fluent 2020 R1 was the main software used, as the company has history of using various other products from ANSYS. Software employed for the current thesis work is presented in the **Table 5**, with their respective uses.

One other strong reason to use ANSYS Fluent was that, integration of user defined functions (UDF's), to determine the flow turbulence and other case specific boundary conditions, in the future is simple and comparatively easier to other commercial CFD software.

Software	
Geometry generation-	<b>Design modeler</b> and <b>Spaceclaim</b>
Meshing-	<b>Workbench Meshing tool</b> and <b>Fluent mesher</b>
Solving-	<b>ANSYS Fluent 2020 R1</b>
Post-processing-	<b>CFX Post-processing tool</b>
Data analysis-	<b>MATLAB</b> and <b>Python</b>

**Table 5: Software used in the numerical model building**

### 3.2.2 CFD domain

The domain of interest in this project is the test space volume of the climate chamber (excluding doors, lights, radio and anemometer mounting stands) of volume about  $3*3.6*4.02 \text{ m}^3$ , in which the electronic equipment would be tested for temperature reliability tests. **Fig. 12** shows the three-dimensional geometrical model of the climate chamber. The pink coloured volume in **Fig.12** represents the fluid(air) inside the control volume present in actual climate chamber. This CAD model was initially developed in Design modeler and later on switched to ANSYS Spaceclaim software. Switching to Spaceclaim came with many advantages such as ease in modeling complex geometry, more user interactive commands and integrated tools to clean up geometry to facilitate meshing. One more important aspect is to establish *Dynamic similarity* between the actual climate chamber and the 3-D model.

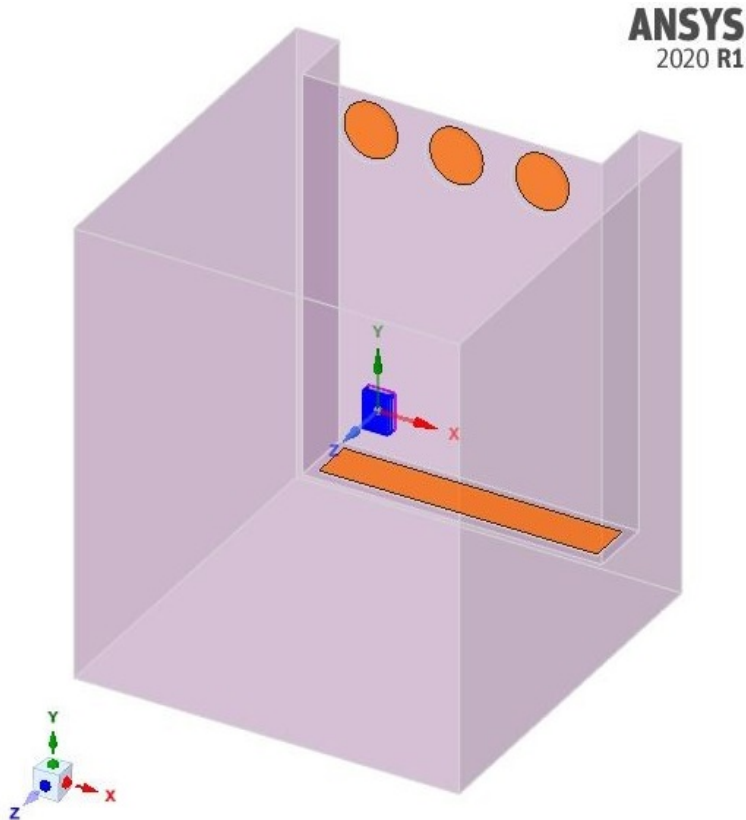


**Figure 12: CAD model of entire climate chamber test space volume with simplified inlet, outlets and mock-up radio unit**

The detailed CAD model of the dummy radio unit was provided by the company, which was developed earlier during the prototype development stages. However, accurate detailing in the radio unit model proved troublesome in meshing as it had many sharp edges and curves. Simplification to minimal extent (removing the smaller round-offs and tapers lesser with radii or taper width less than 5 [mm]) was made to the CAD model of radio unit by not altering the overall shape and dimensions of it, as presented in **Fig. 13 (b)**. There was no scaling (scale-up or scale-down) in size was made in constructing CAD model.

The climate chamber model and the dummy radio unit is symmetric about the YZ-axis as presented in **Fig. 13 (a)**. Symmetry can be worthful in reducing the number of mesh elements by half (or quarter depending on the case) for any considered domain, thereby reducing the computational effort. The effects of symmetry consideration will be discussed in detail in the following sections.

Outlets and Inlet in the CAD model of climate chamber are of vital importance in the numerical model construction, as the boundary conditions specified to these have direct impact on the results. Outlets, as explained earlier are ducts consisting of exhaust centrifugal fans as shown in **Fig. 14**, that suck in air and pass it on to the heat exchangers. These ducts are covered perforated mesh kind of filters (an Aluminium plate of about 10 [mm] thickness, with circular holes of uniform radius, which would avoid sucking of larger foreign substances from the test space volume), that possibly straighten and divide the incoming flow thin streams of air. On the other hand, inlet, is a rectangular opening,

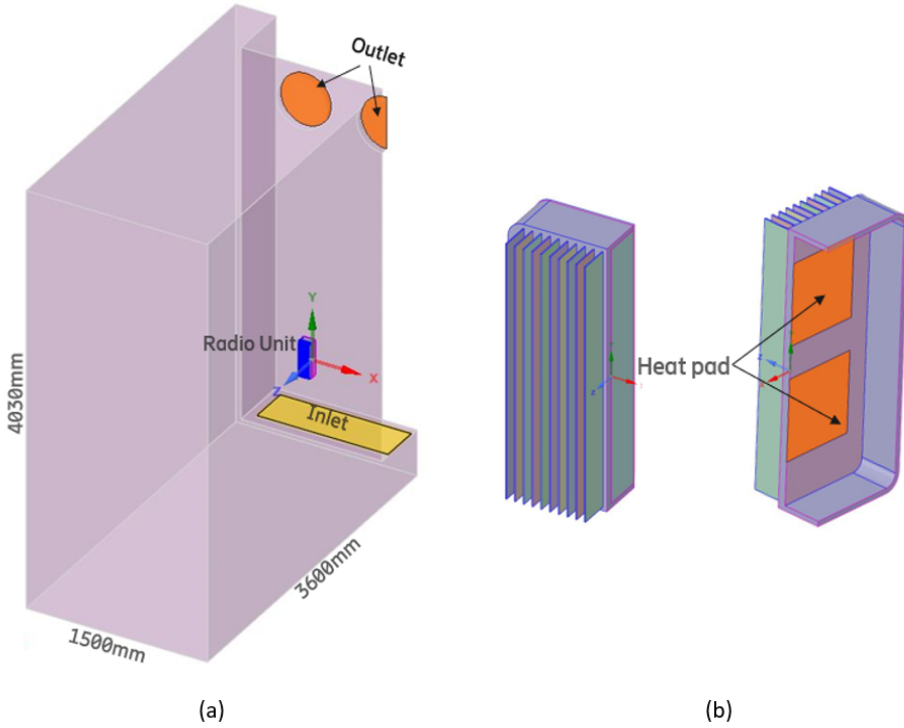


**Figure 13:** (a)Geometry, with symmetry considered and (b) Radio unit with heat pads

facing the floor of about 40[cm] wide, covered with the same perforated mesh (sheet with many rectangular holes). These inlets and outlets were modeled to be flat plate, from which the air would be forced in and out respectively, as the detailed modeling and measurement of the flow conditions (turbulence intensity levels, effect of mesh on the flow, effect of centrifugal fans) in detail are out of the scope of this thesis project. However, the flow is sensitive to inflow conditions at the inlet, but as the flow moves away from the inlet, these effects of inflow conditions have impact to consider them in the calculations.[39] The small volume around the radio unit (at the centre of the test space volume), covering the 4 anemometers as shown in **Fig. 9** is of concern here.

### 3.2.3 Meshing

Meshing is an integral and critical part in CFD modeling. Meshing has a greater influence on the convergence of the solutions, numerical diffusion, and to a notable extent on the accuracy of the results generated. ANSYS Fluent 2020 R1 uses Finite Volume Modeling approach, where the domain of interest is discretized or divided into small volumes. The governing equations are then solved at each of these volumes, thereby predicting the flow physics.

The 3D CAD model of the climate chamber and the dummy radio unit were imported into the meshing tool. Meshing is carried out using ANSYS meshing tool. This choice was made as it provided greater control over mesh generation and was already integrated in ANSYS workbench (where the geometry was developed and further simulations are run), thereby providing a systematic flow, in which a CFD problem is solved. The material properties are already defined during geometry generation phase, aiding the meshing

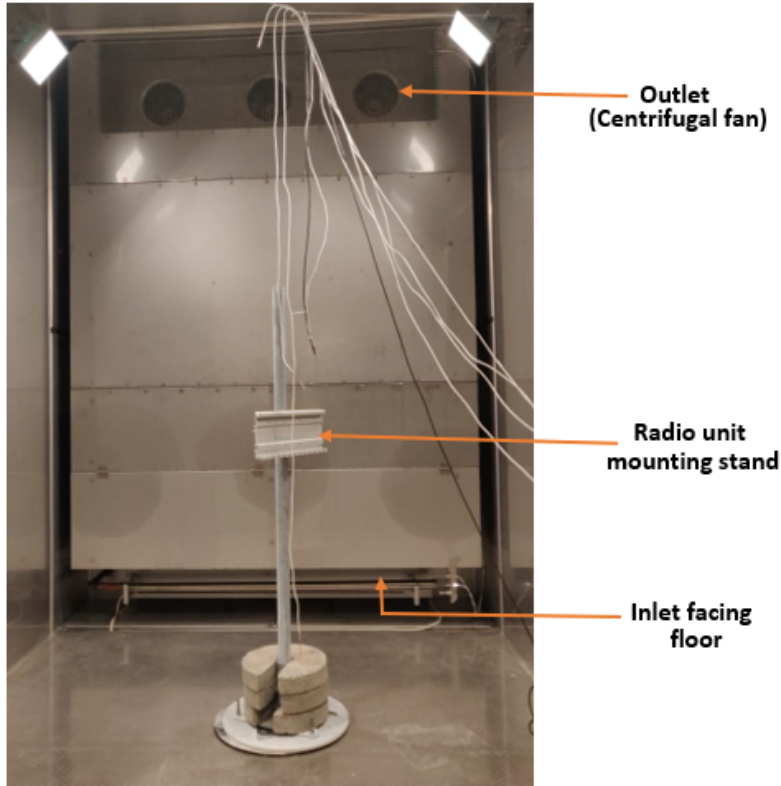


**Figure 14:** Front view inside the climate chamber showing inlet, outlet and radio unit mounting stand. The perforated mesh kind of structure ahead of the three centrifugal fan ducts at the top can be visualised

process. Important mesh controls, such as the growth ratio (1.2), average element size, initial boundary layer cell thickness, no. of inflation layers are set based on trial and error method, in-order to obtain smooth transition when the mesh element size increases gradually and keep the maximum cell count within desired values.

As mentioned earlier, the volume around the radio unit needs mesh of larger density so as to capture physics involved effectively. Heat transfer and other flow phenomena like separation, re-circulation and vortex stretching are expected in the sharp edge corners, which needs to be looked onto with much care. The cells closer to the radio unit have thickness of about 4[mm]. The fluid (air) and solid (Aluminium casing) needs smoother blending in the mesh element sizes, such that there is no dramatic increase/jump in the consecutive elements size. Face sizing and edge sizing features are used to match the meshing at the interface (solid-fluid) regions. The maximum element size in the domain is set to 35[mm].

Body of influences are modeled around the radio unit, inlet and outlets as presented in **Fig.15**. This is done to increase the density of the mesh or have a finer resolution around these complicated areas. 10-15 inflation layers (number of layers obtained by trial and error basis, to keep the wall Yplus closer to 1, with an intent to model heat transfer at the walls effectively) are used in the fluid and solid interfaces (along the walls), to resolve the boundary layer. The wall yplus value is resides closer to 1 in all the regions, satisfying the requirements for wall modeling. Current mesh has 2.1 million mesh cell elements and is presented in **Fig.16**

**ANSYS**  
2020 R1

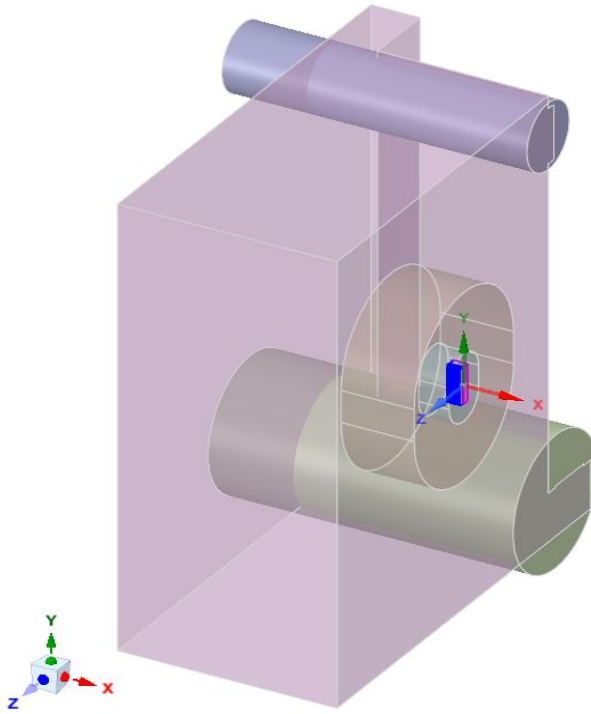


**Figure 15:** Body of influences generated at complex areas to increase the density of the mesh in such areas, thereby capturing physics effectively in the critical regions

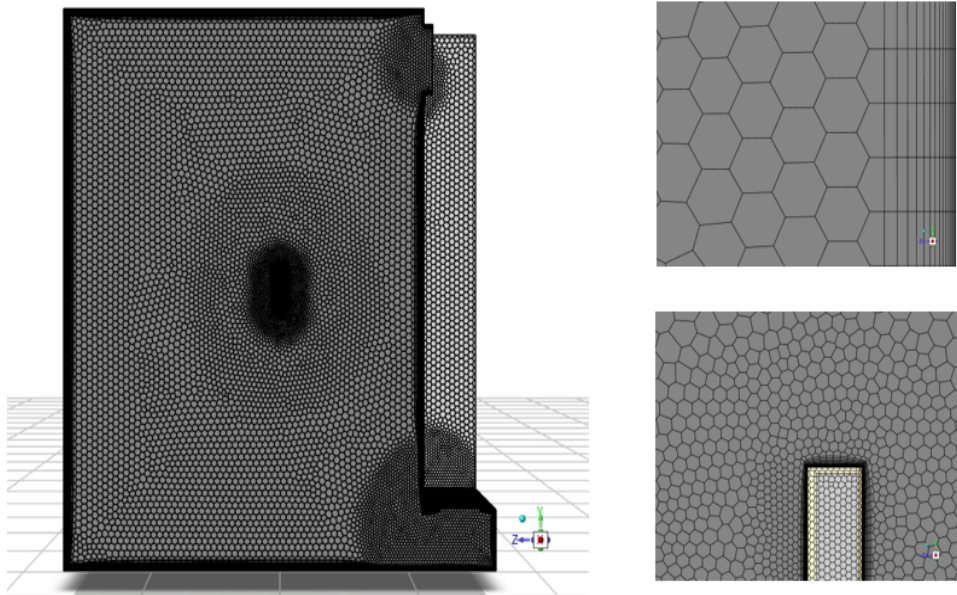


**Figure 16:** Generated mesh consisting of polyhedral cell elements and the inflation layers at the walls. The transition from the cells closer to the wall to far away region is smooth, such that there is no sudden jump in the size.

The quality of the generated mesh is checked using the mesh metrics such as Skewness, Orthogonality, Aspect ratio and element quality. The quality of the final mesh gen-

erated is presented in the **Table.6**, with the maximum cell quality 1. A cell convective Courant number of 0.25 is maintained (from previous studies conducted at Ericsson AB), so as to capture the information effectively. Grid adaptation tool is used to check the cells that have very high courant numbers, and then the mesh in those areas are coarsened by not affecting the overall element quality. The time step size of 0.005 [sec] is maintained so as to keep the courant number closer to 0.25 in the entire chamber and particularly in the volume of interest. Also, the grid adaptation tool is used to mark the cells that have low mesh quality or have mass imbalance, without making any adaptations and later necessary steps like refining or coarsening the cells is done to improve the situation. **Fig.17** shows the cells that have element quality less than 0.75. These cells are then refined to improve the cell quality.

Mesh Region	Maximum mesh quality	Cell count
Radio unit cover	0.951	1185
Radio unit core	0.795	4094
Radio unit heat-sink(Fins)	0.987	9577
Air	0.963	1791115

**Table 6: Mesh metrics for mesh quality control**

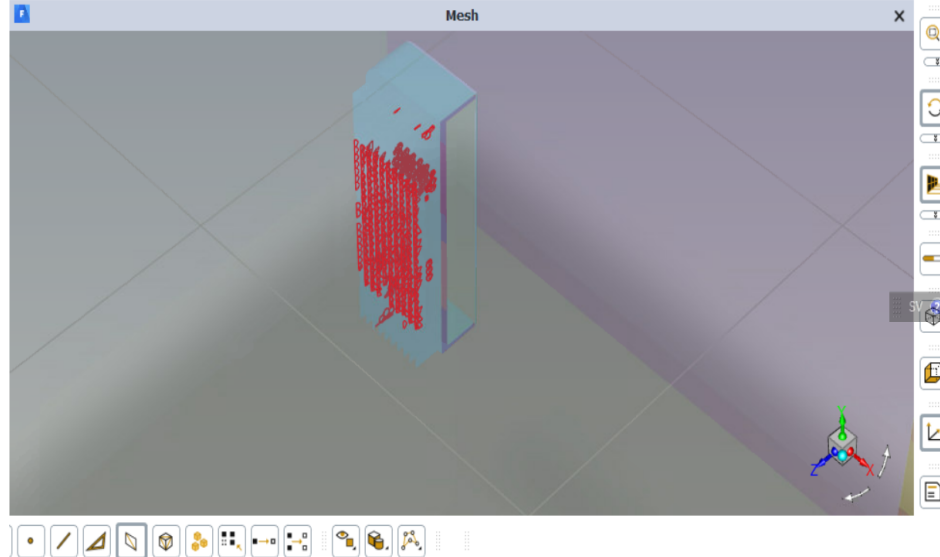


**Figure 17: Mesh cells that have cell quality less than 0.75 are marked as the red cells**

### 3.2.4 Mesh Independency studies

Current case setup is a laminar case, where no turbulence model is employed to model / predict the nature of flow, instead the numerical equations are directly solved. Here, the larger eddies in the flow are directly resolved and the smaller eddies are not modelled using any turbulence models (which require a large amount of computational resources to

resolve and model as well). Henceforth, determining a optimum mesh cell count makes no sense. The finer the mesh gets, the more is the detailing in the model. The larger eddies are of greater interest here (though some of the smaller eddies must be captured), as these eddies contain most of the turbulent kinetic energy and are easier to resolve than the small scale eddies where the kinetic energy is lost in the form of heat dissipation by energy cascade. These larger eddies are flow dependent and are highly anisotropic in nature.

However, to have certain upper end limitations on the mesh cell count, 'LES best practice guidelines' documentation was used.[24] (Slide 13). In order to resolve around 90% of turbulent kinetic energy present in the flow, it is a good practise to have at least 12.5 cells (approximately 10-12 cells) have to placed across integral length scale,  $L_0$ . This brings in a requirement of 12.5 cells or approximately 13 cells to fit in along the length of the integral length scale.[24] (Slide 13) And to capture 80% of turbulent kinetic energy, approximately 4-5 cells have to placed across integral length scale,  $L_0$  [24] (Slide 14). This summarizes that the minimum edge length in the mesh generated is about  $L_0/5$  units to resolve 80% of turbulent kinetic energy.

### 3.2.5 Boundary conditions

**Velocity inlet boundary condition** is specified for the inlet with the magnitude and direction. The magnitude of inlet velocity was initially decided to obtain by means of physical measurement at the inlet ducts inside the climate chamber by using hand-held anemometers. Due to the wider area to the inlet duct and limited availability of the climate chamber access, physical measurement was not possible.

As an alternate solution to the newly aroused problem, trial and error method was adapted to match the radio unit temperatures (which were recorded experimentally using thermocouples at different fan speed settings) with the temperature readings that were obtained from the probes placed around the heat pads in the numerical model. These probes are placed on the CAD model of the radio unit in the exact locations as they were placed on the physical radio unit as shown in **Fig.18**. Different inlet velocities were specified to the numerical model within a range of 0.5 - 2.5[m/s] with an increment of 0.5. Each time the temperature readings of probes from the transient simulations were averaged and compared against the experimental data. When the inlet velocity for the numerical model was set to 1.5 [m/s], the temperature readings of the probes matched with the experimental temperature readings that were recorded at 50% fan speed. Henceforth, the inlet velocity magnitude for the numerical model was finalized to 1.5[m/s].

The turbulent intensities and the eddy viscosity ratio at the inlet plays an important role in determining the inflow to the climate chamber. As explained earlier, these conditions have minimal effects at the region away from the inlet (which is the context here). Accurate measurements and calculations of turbulence parameters at inlet and outlets would be more time consuming, considering the scope of the thesis.

**Pressure outlet** is set at the outlet surfaces. Mass-flow rate boundary condition is an alternative to the pressure outlet to be specified at the exhaust fans of the climate chamber. However, a specific value of the mass-flow rate had to be specified at the outlet, which can induce errors when other boundary or operating conditions are tweaked.

The operating temperature is the ambient temperature of 25[°C] and operating pres-

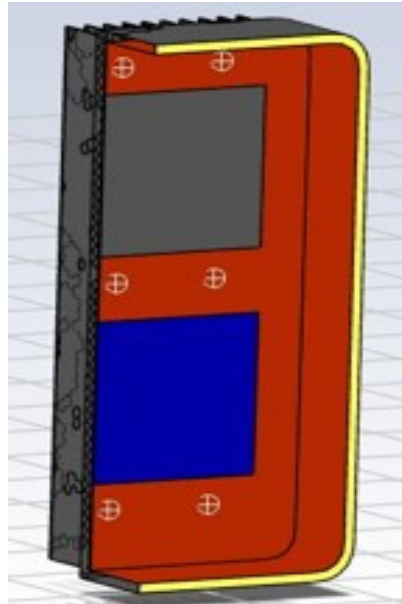


**Figure 18:** Temperature probes on the CAD model of the radio unit, indicated by white crossed circles. The grey coloured rectangle indicates the top heat pad and the blue coloured rectangle indicates the lower heat pad

sure of 101325[Pa]. Boussinesq approximation is in the density setup and an operating density of 1.1839 [Kg/m<sup>3</sup>] is used. Both the inlet and outlet were also set at 25[°C] of operating temperatures.

The two heat pads presented in Fig.13 are specified **heat flux** values, so that they act as the heat sources. The upper heat pad is supplied with voltage of 18.44[V] and 8.16[A] of current. And the lower one is supplied with voltage of 10.52[V] and 4.96[A] of current, so that they generate 150 and 50 Watts of heat respectively. The heat fluxes values of 7500 [KW/m<sup>3</sup>] and 2500 [KW/m<sup>3</sup>] are specified for top heat pad and bottom heat pad respectively. All other walls (walls of the climate chamber) are set as **no-slip walls** and the symmetry condition is used for the plane where symmetry is generated. The boundary conditions that are specified in simulations are indicated in the Fig.19.

### 3.2.6 Solver setup

In the solving stage of the CFD problem solving, the iterative solver is tuned necessarily according to the required specifications. As the velocity of air flow inside the climate chamber is subsonic (around 1.5 [m/s]), **Pressure based solver** is used. Density based solver is used when the compressibility effect on the fluid is not negligible. When the Mach number of the fluid flow is less than the 0.3, the flow is considered to be incompressible, where the density of fluid is assumed to be constant. Modeling of heat transfer through natural convection from radio unit to the surrounding air is the major aspect that the numerical model has to emulate to closest possible extent as determined from the experiments inside the chamber. Conservation of energy is achieved within the test space volume. Energy equation is primarily responsible for the heat transfer modeling in a fluid dynamics problem. Gravitational force (acceleration due to gravity, with the value of 9.81 [m<sup>2</sup>/s]) is specified as the buoyancy force is an important parameter in the

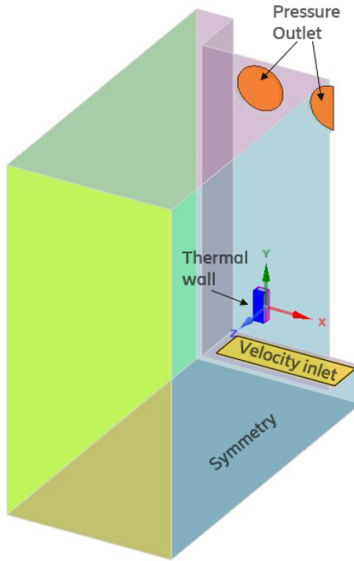


**Figure 19: Specified boundary conditions in the simulations. The walls that have no name indications are specified as no-slip walls**

natural convection phenomena.

**SIMPLE** (Semi-Implicit Method for Pressure Linked Equations) algorithm is used for the iterative method of solving by the solver. This algorithm is used for the purpose of introducing pressure variable into the continuity equation. The main advantage of this scheme is due to the reduced effects of the pressure corrections onto velocity in the velocity correction equations.[40] In the laminar simulations the convergence is limited by the pressure-velocity coupling. Employing SIMPLE scheme would help to reduce the computational time by attaining the convergence quickly than other schemes (as the velocity correlations are better).[40]

**Second order upwind scheme** are used for the discretization of Momentum, Energy and Discrete Ordinates (From the radiation model). This scheme is simple (less complex, not to be confused with SIMPLE algorithm) in nature and more stable than the first order schemes, as more points are being used in the computation of the flux parameters.[12]

Default values of under relaxation factors (URFs) are used. For the radiation model, Discrete ordinates is used to consider the heat transfer by radiation, that is emitted by the radio unit. This choice is made from the usual practice that is followed by the company during running similar simulations previously. The solver settings are summarized in the table presented below in **Fig.7**.

About 20 iterations are specified per time step during the solving process. This done with an intention to make the residuals drop by two orders of magnitude (per say from 10-4 to 10-6) when the solution is being calculated. (Used as a general thumb rule for similar works at Ericsson AB) This ensures that the error gets sufficiently low to proceed for further time step. Convergence criteria is one another important parameter to keep a check on during the solving process in order to obtain better results. Residual value convergence is a direct measurement of the error in the solution of the equations that are solved in an iterative manner. It measures the local imbalance of the flux parameters between the consecutive iterations.

In the simulations set up here, a specific value of convergence or relative tolerance

### Solver settings

Simulation type-	Unsteady simulations
Turbulence mode-	Laminar model
Energy equation-	Enabled
Radiation model-	Discrete Ordinates
Under relaxation factors-	Pressure→ 0.3 Density→ 1 Body Forces→ 1 Momentum→ 0.7 Energy→ 1 Discrete Ordinates→ 1
Pressure-Velocity coupling-	SIMPLE scheme
Discretization scheme-	Momentum→ Second order Upwind Gradient→ Least Square Cell Based Pressure→ Body Weighted Average Energy→ -Second order Upwind Discrete Ordinates→ Second order Upwind Transient formulation→ Second order implicit
Time step size-	0.005 sec
No. of iterations per time step-	20 iterations

**Table 7: Solver settings, discretisation schemes and parameters defined during the simulation setup stage**

between the consecutive iterations is not specified like it is usually done as a general rule of thumb. Though it is known that, the lower the value of the relative tolerance, the solution is more numerically accurate, the convergence values are not strictly checked.

Instead, the steady state of the residuals is preferred, where there is no convergence or divergence in the residuals vs iterations/flow-time. The fluid flow problems are highly nonlinear in nature, that needs some kind of restricting conditions in order to solve the Navier-Stokes equations numerically.

A steady state solution is lot worthier than a solution that has fluctuating residuals even though the convergence criteria is satisfied. The residuals for the case where symmetry is considered in the domain are presented in **Fig.20**. The residuals here drop three orders of magnitude for every time step (20 iterations for times step). Convergence studies are necessary for verification of the results that are generated. Setting up monitors at important locations in the domain and monitoring the flux parameters is also a good technique in the convergence studies. Residuals of Mass flow rate at the outlets and inlet section is being monitored in the simulations here. The monitors for the mass flow rate at the outlet are presented in **Fig.21**. It can be seen that the value of the mass flow rate stabilizes for a value of -0.92 [Kg/s]. So the mass of air flowing or removed through the outlets is constant. **Fig.22** presents the velocity variations recorded by the monitor points located between the radio unit and the front anemometer. This ensures that the flow is fluctuating in the domain and varies within the same range of velocities as the experimental results for 50% fan speed. However, the comparison is not accurate enough, as the experimental data is enormous, of about 45 minutes and the numerical data is of 6 seconds long. The temperature monitor plots presented in **Fig.23** show the variations recorded by the temperature probes. The straight lines parallel to the x-axis are not exactly straight, but slightly fluctuating in nature. These fluctuations are comparatively smaller (these are the temperatures logged by probes located around the heat pads) to the fluctuations recorded by the probes located above the radio unit (green, black and red lines).

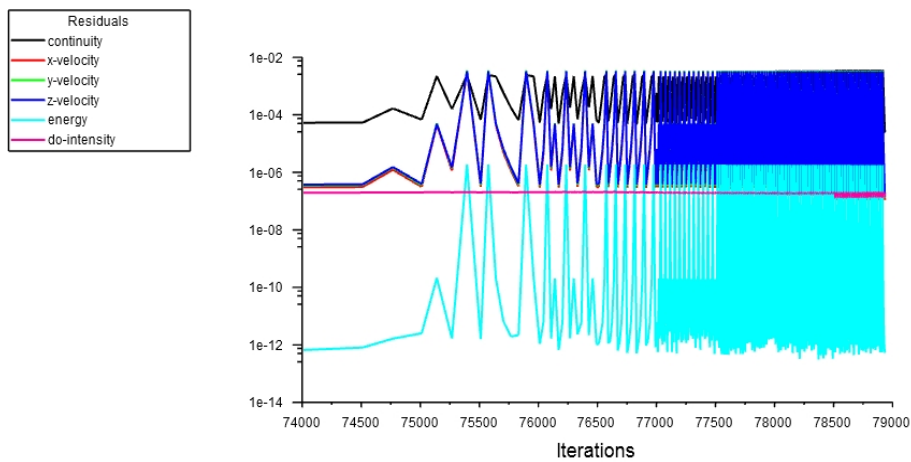


**Figure 20: Residuals for the case with symmetry approximation for the domain vs the number of iterations graph**

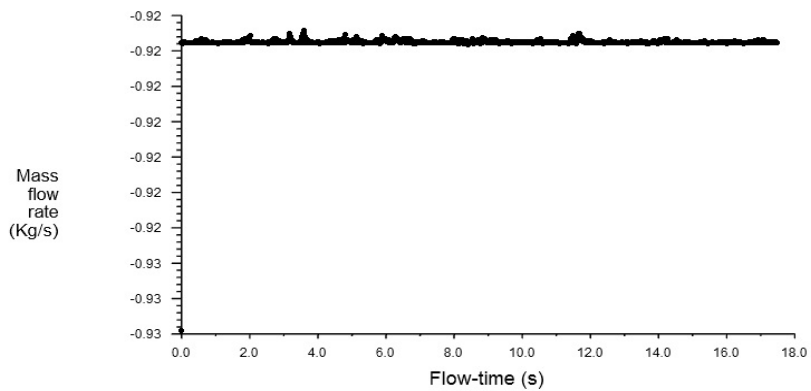


**Figure 21: Mass flow rate at the outlet (all three exhaust ducts combined) vs flow-time graph**

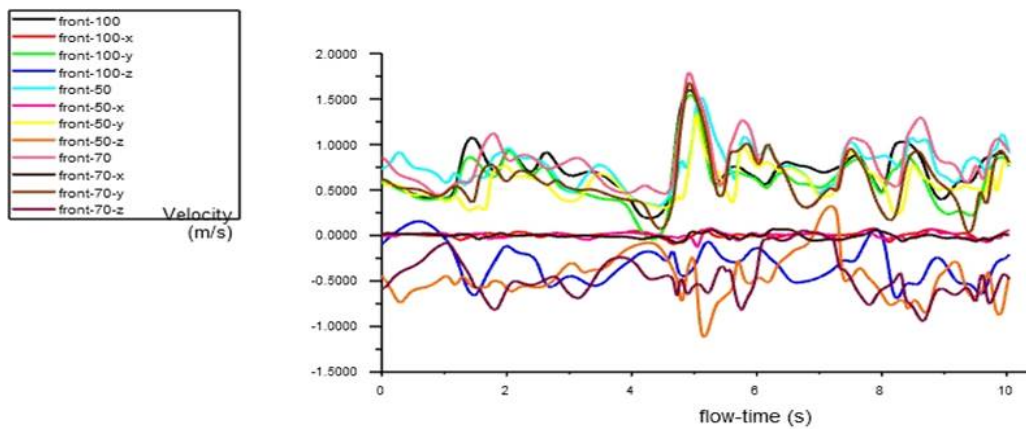


**Figure 22: Velocity monitor point plots plotted with sampling time. These monitor points are located at the same location as the anemometer's placement between the front door and the radio unit**

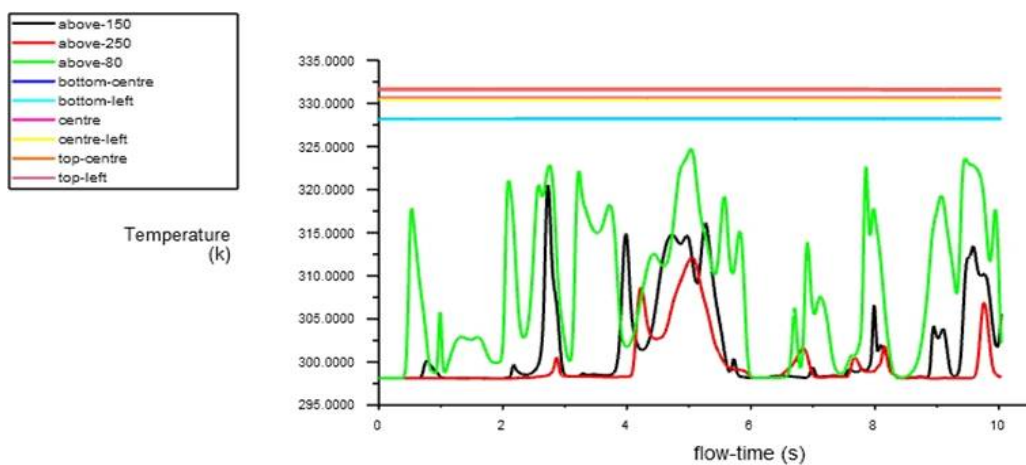


**Figure 23: Temperature monitor plots, obtained from the temperature probes that are placed inside the radio unit and around the radio unit.**

### 3.3 Post-processing procedure

The post-processing of the velocity data obtained from the experimental and numerical simulations were done systematically as depicted in the **Fig.24**. Analysis of velocity data is done, with an aim to plot the turbulence spectra. From this turbulence spectra, the length of the largest scales present in turbulent fluid flow inside the test space volume is determined, which would serve as a parameter to compare numerical and experimental data.

The velocity data obtained from ultrasonic anemometer and velocity probes (simulation data), is plotted in a graph with time as the abscissa and velocity as the ordinate. The longitudinal velocity component is considered for further analysis, as these values represent the behavior of the flow. Also, the direction of the anemometer placement, in which the axis is pointing is parallel to the circulation of air inside the test chamber. The longitudinal component corresponds to the  $U$  axis in **Fig.(3)**. This axis is represented physically by the north sign (N) engraved on the anemometer. The total velocity components are then separated into mean and fluctuating components of velocity using Reynold's decomposition technique in MATLAB. The fluctuating components are of importance here, which would be used for further processing. Fast-Fourier Transform (FFT) of this velocity vs time is computed, so as to convert it into velocity vs frequency domain. FFT results in a mirror image of graph containing real and imaginary values. The positive part (real numbers) is considered, as the graph is symmetry along the Y-axis. This FFT is computed or plotting using a MATLAB built-in function.

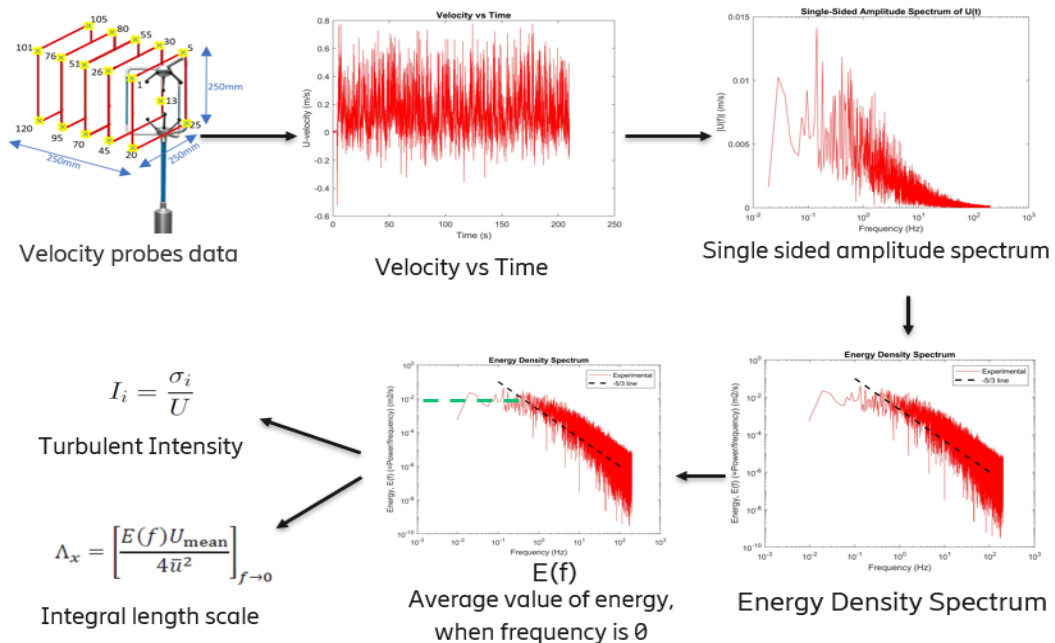


**Figure 24:** Post processing procedure for the numerical and experimental velocity data

From this Fast Fourier Transform, the Power Spectral Density (PSD) of the fluid flow is obtained. This PSD is plotted using a MATLAB inbuilt algorithm known as the Welch (PWELCH) algorithm. This algorithm is fed with the velocity signals and the sampling frequency. The windowing or filtering is not altered as the details of the values of the

constants that are valid in this particular case were unknown. Digital signal processing is another domain which is very vast, and it would be a diversion from the topic if detailed filtering of the signal is considered. The result of PWELCH algorithm is a spectral density plot with the Spectral energy in the ordinate and the frequency as abscissa.

Integral length scale in the turbulent region is the characteristic length of the largest eddy present in the turbulent zone, as explained earlier. These scales are measurable (from empirical formulae **Eq.19**, and auto-correlation techniques) and characterize the distance over which the fluctuating component of velocity of the flow is effective or in other words correlated.[11]. The value of the length scale is calculated using the formula **Eq.19**, presented in [9], which was originally developed by Roach [10].

$$L_o = \left[ \frac{E(f)U_{mean}}{4\bar{U}^2} \right] \quad (19)$$

Here,  $L_o$  is the Integral length scale,  $E(f)$  is the spectral energy when the frequency  $f$  tends to zero and  $\bar{U}$  is the standard deviation of the U-component of velocity. The value of  $E(f)$  is computed by taking the average of first 100 values the spectral energy function,[9] that is computed from the ratio of Power (Fast Fourier Transform) and the sampling frequency.

Calculating the turbulence intensity of the incoming flow at the inlets of the climate chamber, helps in determining the boundary conditions for the numerical model. Turbulence intensities represent the intensity of wind fluctuations, it involves the mean wind speed and the standard deviation of these wind fluctuations,[12] and are represented in the expression as follows:

$$I_i = \frac{\sigma_i}{U} \quad (20)$$

In **Eq.(20)**,  $I$  is the turbulent intensity,  $i$  is the longitudinal component of fluctuating wind speeds,  $\sigma$  is the standard deviation of the fluctuating wind speeds,  $U$  is the mean velocity or the Reynolds average of the velocity. The standard deviation can be computed in fluid dynamics as the root-mean-square of the turbulent velocity fluctuations.

### 3.3.1 Averaging numerical data

The spectral analysis is performed only for one position of the anemometer, where the anemometer is placed between the front door and the radio unit, though there were three other positions of the anemometer as depicted in **Fig.25(a)**. This position, indicated as 'Front velocity probe in **Fig.25(b)**', is quite interesting to analyze as there were no obstructions like the wires from the radio unit. Thermocouples, wires and arms of the mounting stand which were present in other positions and would disturb the flow. The aim is to match the experimental setup in the simulations, thereby avoiding discrepancies to every possible extent.

The exact position of the anemometer, in terms of the height from the floor and distance from the radio unit is unknown (Unavailability of access to the climate chamber due to Pandemic situation). To solve this problem and also to bring in some kind of filtering or averaging to the numerical data, there were many probes placed around the anemometer head ('Fixed position'). The 'Fixed position' in **Fig.26** indicates the approximate height of 1.5[m] from the floor and 0.8[m] away from the radio unit. An imaginary

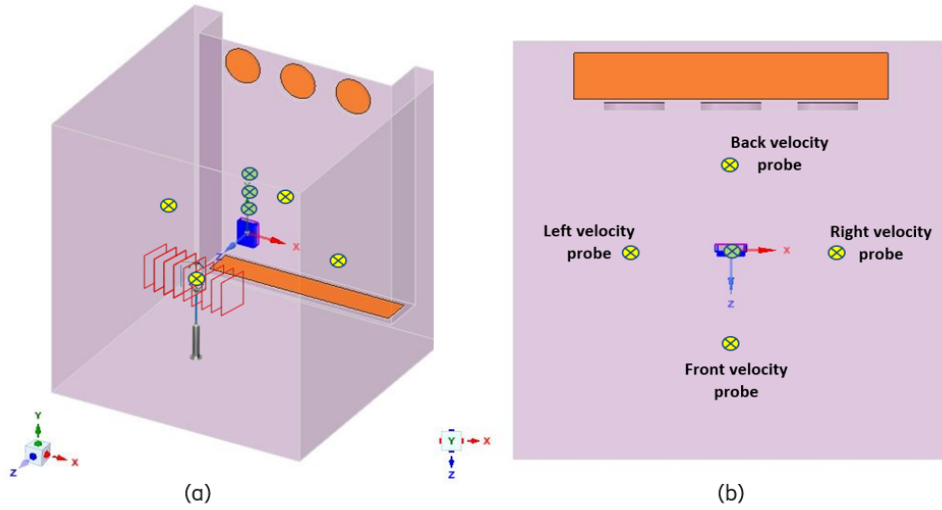


**Figure 25:** (a) Iso-metric view and (b) top view of the climate chamber geometry model, indicating the velocity probes (yellow crossed circles) and temperature probes (green crossed circles), with the radio unit in the centre in blue colour

cube is placed at the 'Fixed position', in which the probes are placed at equal distance. The velocity data at these probes are then logged during the simulations and then averaged effectively to reach a single value at every time step. The number of probes required was calculated from the Eq.21.

$$\text{Number of Probes} = \frac{\text{No.ofSamplesInExperimentalData}}{\text{SamplingFrequency} * \text{FlowthroughTime}} \quad (21)$$

The experimental data was recorded for about 38 minutes, with a sampling frequency of 20 [Hz]. This would give a data set of about 46000 samples. On using these values in Eq.21, we get the total number of probes to be 128. For simplicity and easier calculations, 125 probes are spread out around the initial position of the anemometer in a cube of side 250[mm]. The probe locations are presented in the Fig.26 (a). Each layer consists of 25 probes. And for the non-symmetry case, 225 probes are used as depicted in Fig.26 (b) to the right.

The velocity data is extracted at every probe and then the turbulent kinetic energy is calculated for each probe throughout the duration of the sampling time. Later on a cumulative average of 125 probes is computed for the turbulence kinetic energy and the energy spectral density graph is plotted against frequency.

The green crossed circles depicted in Fig.25(a), are the temperature probes that are located right above the centre of the radio unit at 80 [mm], 150 [mm] and 300 [mm]. These probes are placed to check if the heat is flowing out of the radio unit by natural convection. The farthest probe located at 300 [mm] above the surface of the radio read temperature closer to ambient conditions, whereas the closer probes read higher temperatures due to the influence of the heat flowing from the radio unit.

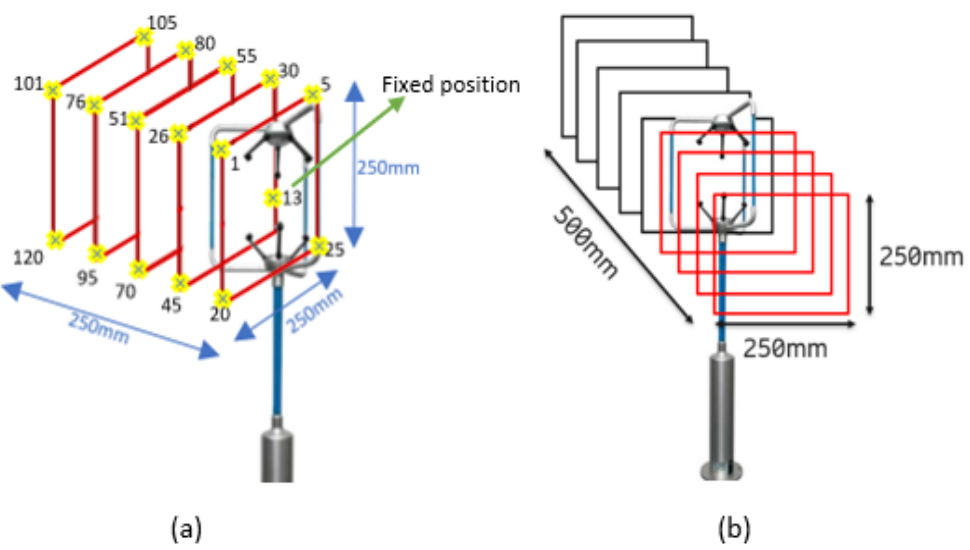


**Figure 26: Probes distribution around the anemometer for symmetrical (a) and non-symmetrical (b) case. These probes are numbered from 1 to 125, which log x, y and z components of velocity in all three directions**

# 4 Results

This chapter presents the results that were developed from the post processing of data from experimental and numerical techniques.

## 4.1 Experimental results

In this section, the results obtained from experiments inside the climate chamber will be presented in the chronological order as they were conducted. The relevance of these results in this project work as well as their importance of these will be discussed in the upcoming chapter. Though temperature and velocity readings were extracted for 3 different fan settings speeds (30%, 50% and 100%), the focus is laid on the 50% fan speed setting, which will be used for comparison against the data from the numerical simulations.

The **Tab.8**, presents the steady state temperature readings of the thermocouples. The thermocouple locations are indicated as 'sensor' in the table, that are placed around the heat pads, replicating the same locations as presented in the Fig.8. The variations of the temperatures are presented in the **Fig.27**

	Sensor 1 °C	Sensor 2 °C	Sensor 3 °C	Sensor 4 °C	Sensor 5 °C	Sensor 6 °C
<b>30% Fan speed</b>	65.06	64.38	61.09	60.13	52.02	51.08
<b>50% Fan speed</b>	60.53	59.69	57.38	56.57	48.75	48.76
<b>100% Fan speed</b>	54.58	54.13	52.64	51.70	44.94	44.70

**Table 8: Reference values for the steady state temperatures in the radio unit for 30%, 50% and 100% fan power. The thermocouple sensors provide temperature values accurate to two decimal points**

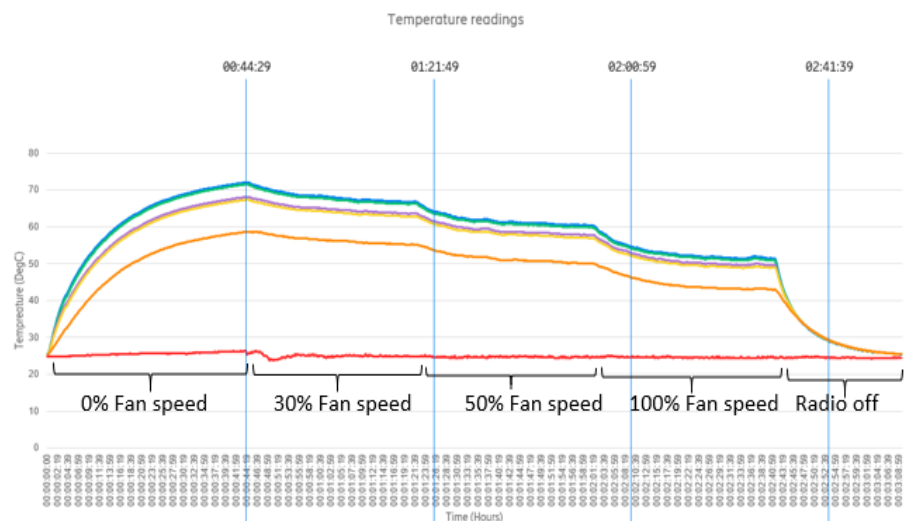


**Figure 27: Variation of temperature with the change in fan speed settings**

The mean wind speed values recorded by the anemometer placed between the radio unit and the front door, represented as 'Front velocity probe' in **Fig.25(b)** is presented as a graph between velocity and number of samples in **Fig.28**. The velocity values were logged at 20[Hz] sampling frequency. Initially the fan power was set to 30% (the first 50000 values correspond to this fan speed), and then increased to 50% and 100% of fan speeds eventually, by not altering the temperature of the radio unit using power supply unit manually.

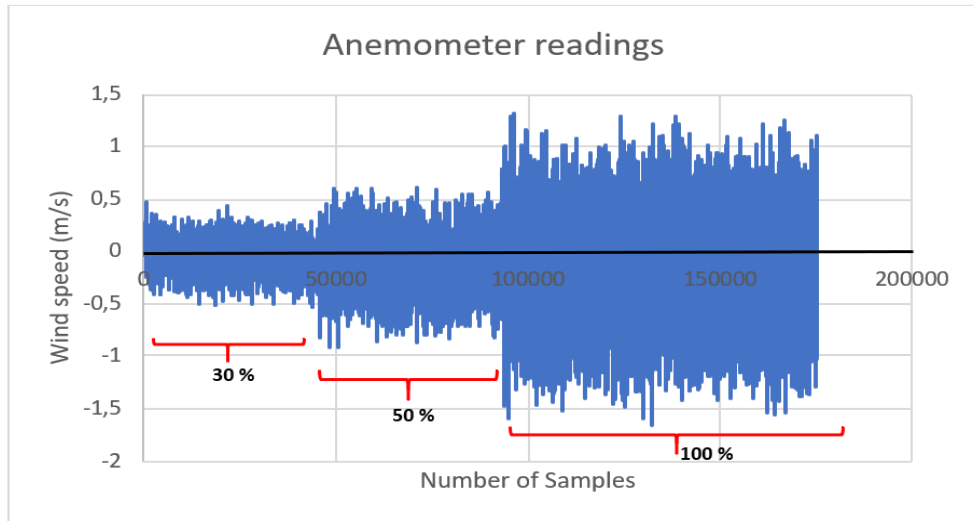


**Figure 28: Anemometer readings when the fins of the radio unit are facing towards the door**

The mean velocities of the air inside the climate chamber surrounding the radio unit can be seen in **Fig.29**. These velocities are not to be confused with the inlet mean velocity at the duct. The velocity at the duct are way higher than the velocities recorded by the anemometers. Mean velocities at three different fan speed settings, recorded by anemometers at four different locations are shown. These velocities have nothing to do with setting up of boundary conditions to the numerical simulations. They just provide an estimate of how energetic (in terms of velocity) the flow is around the radio unit.

To obtain the characteristic speed in the chamber, the wind speed values in the front door position are selected. The motto behind selecting these values is that, this position is free from the interference of wires(thermocouples and the radio unit connections), and other obstacles, thereby emulating close conditions to that set up in the numerical simulations. These values serve as reference for comparisons and are required for further calculations of integral length scales and turbulent intensities. The air coming out of the inlet reaches the front door position first in the flow cycle. The air after hitting the front door comes in contact with the anemometer placed in this position (thereby receiving clean air free from unwanted obstacles) and later on it gets in touch with the anemometers places at other locations.

The single sided amplitude spectrum, as a result of applying Fast Fourier Transform to the fluctuating components of the velocity signals and the Power Spectral Density, obtained by squaring the velocity magnitude is shown in **Fig.30**.

From the Power Spectral Density, the Energy Density Spectrum (EDS), is plotted as shown in the **Fig.31**. this describes the energy distribution in the signal with frequency. However, this spectrum has to be thinned out or filtered in some manner to compare

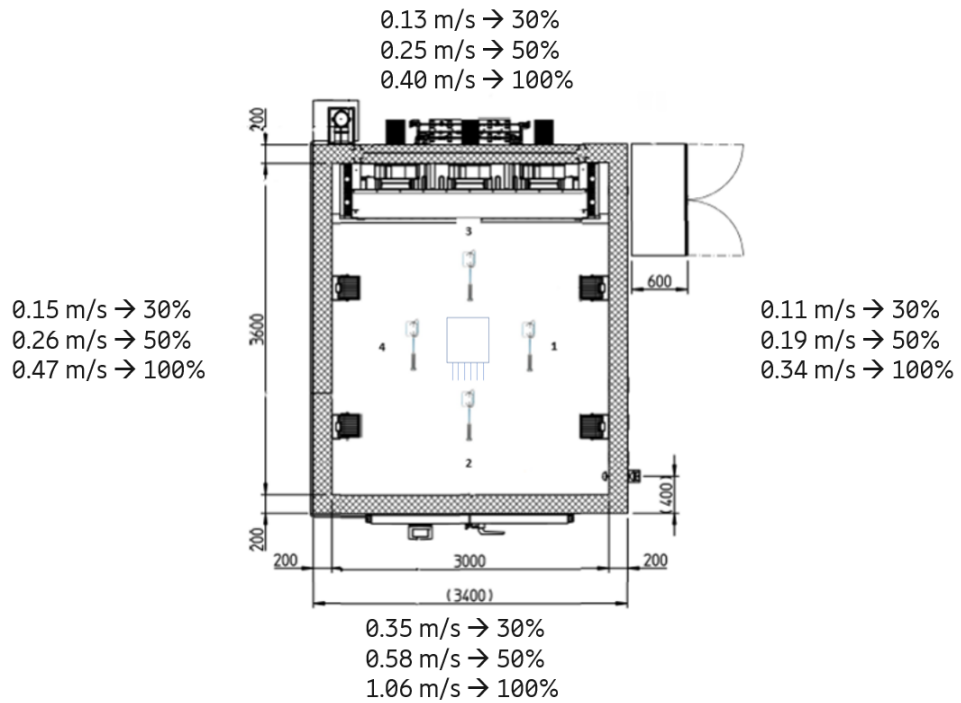


**Figure 29: Mean wind velocities around the radio unit (fins facing towards the front door)**

	Characteristic speed in test chamber [m/s]
<b>30%Fan speed</b>	0.35
<b>50% Fan speed</b>	0.58
<b>100%Fan speed</b>	1.06

**Table 9: Reference values for the steady state temperatures in the radio unit for 30%, 50% and 100% fan power. The thermocouple sensors provide temperature values accurate to two decimal points**

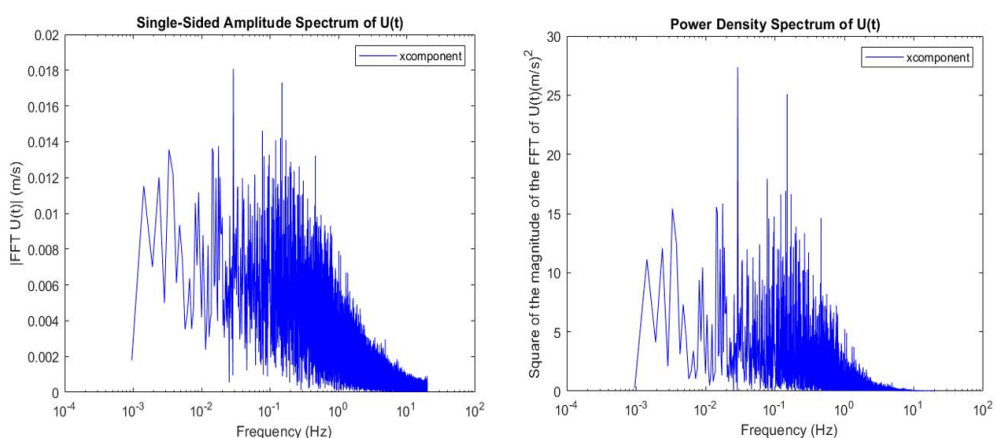


**Figure 30: Single sided amplitude spectrum and Power Density Spectrum of the velocity signals from the anemometer placed between the front door and the radio unit**

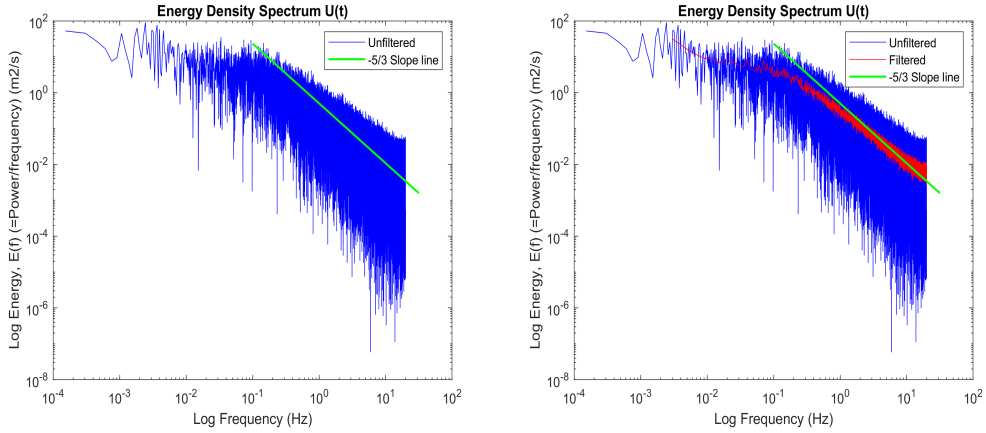


**Figure 31: Energy Density Spectrum of the fluctuating velocity component signals for 50% fan speed configuration and the filtered/averaged Energy density spectrum**

against the -5/3 slope line (indicated by the green line in the figure). This is done by dividing the data set into 20 sets and average of the spectral densities is computed in MATLAB to filter out the spectra and plotted in the frequency domain. The red spectra in **Fig.31** is the filtered out spectra for the experimental set of results

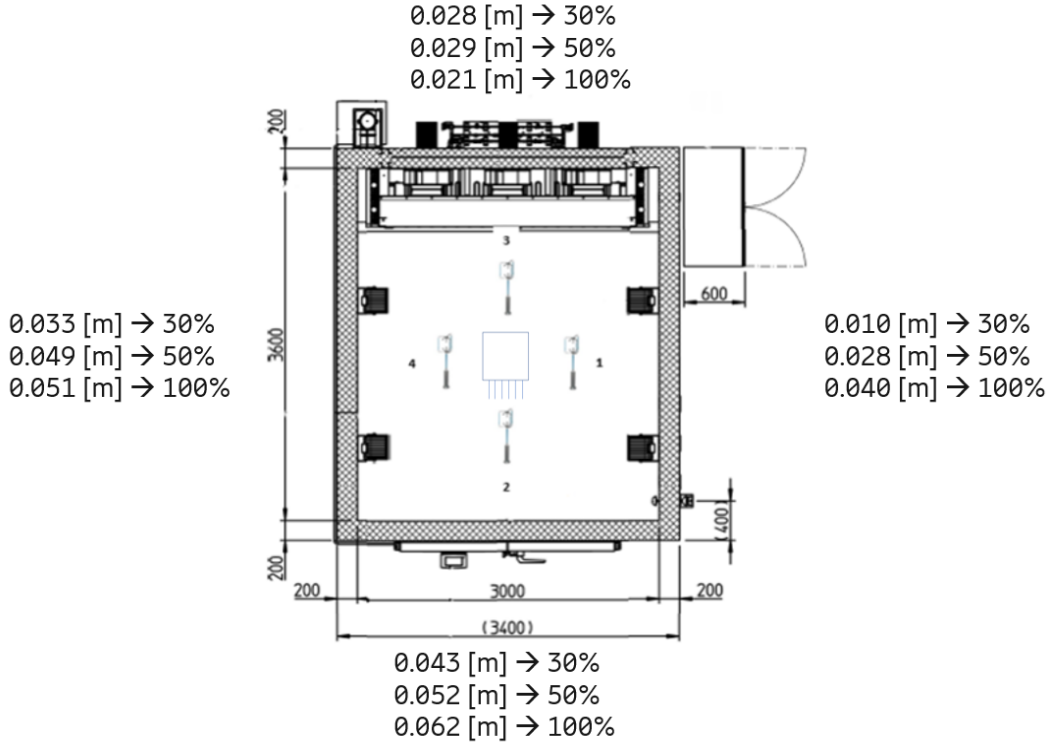


**Figure 32: Integral length scales calculated around the radio unit (fins facing towards the front door) inside the climate chamber for different fan speed settings**

**Fig.32** presents the integral length scales calculated using the Roach's[10] method, from Eq.(19). This parameter will be used in comparison of numerical and experimental data. It can be seen that the magnitude of the integral length scales increases as the fan

speed setting increases. However, this parameter is very sensitive to the obstacles present inside the test space volume.

The turbulent intensities of the flow at the four locations around the radio unit are presented in the **Fig.33**. The turbulent intensity values in red colour corresponds to 30% fan speed setting, yellow colour corresponds to 50% fan speed setting and green colour corresponds to 100% fan speed setting.

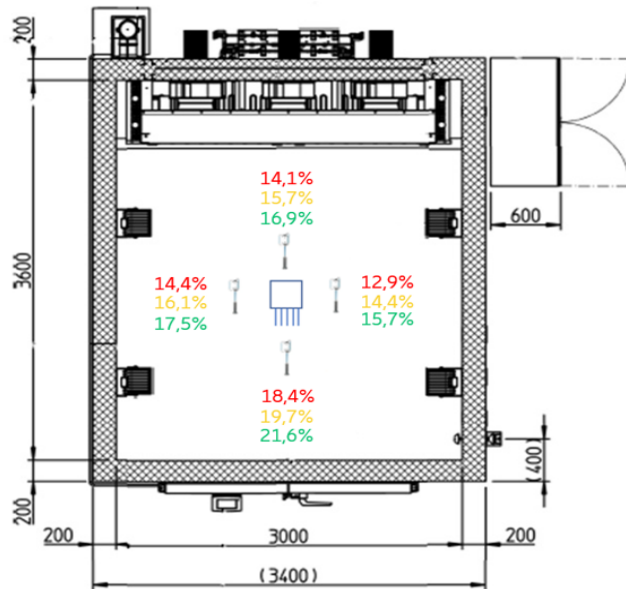


**Figure 33:** Turbulent intensities of the flow around the radio unit (fins facing towards the front door) inside the climate chamber for different fan speed settings

## 4.2 CFD simulation results and comparison

In this section, the results from the baseline numerical model that is built in the ANSYS Fluent software are presented. Some results are compared with the experimental readings and data from other studies (previous studies on the same apparatus at Ericsson AB), that match the studies done during the thesis period. The detailed discussion about the comparisons would be presented in the further sections, which would provide better understanding of the extent to which the numerical model can be trusted for its results.

**Fig.34** presents the temperature flow monitors for the laminar steady state analysis that is used as the initialisation for the transient analysis. The locations of the temperature monitors, above the radio unit can also be seen in the figure. The star sign marks in red, green and black represent the velocity monitor locations (similar to the yellow crossed circles as seen in **Fig.26**), that are placed 0.7[m] from the origin to mimic the locations of the anemometer placements inside the chamber. **Fig.35** shows the temperature probe values varying in the transient simulation runs.

The temperature readings recorded by the experimental studies, previous studies conducted on the same experimental apparatus and the data obtained from the numerical studies are presented in the **Tab.10**

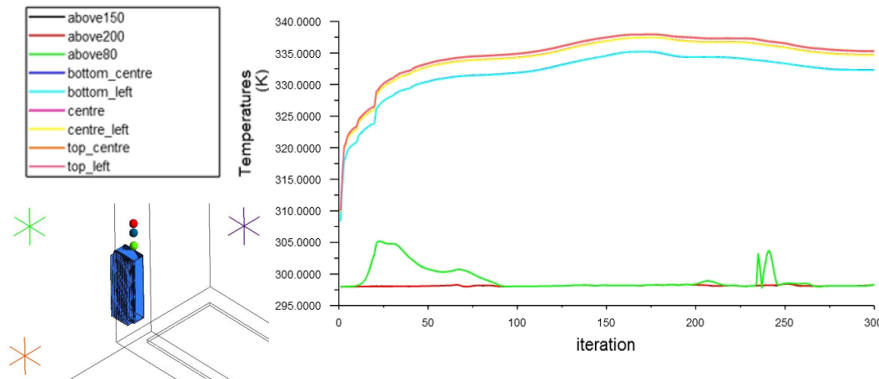


**Figure 34: Temperature residuals of laminar steady state simulations**

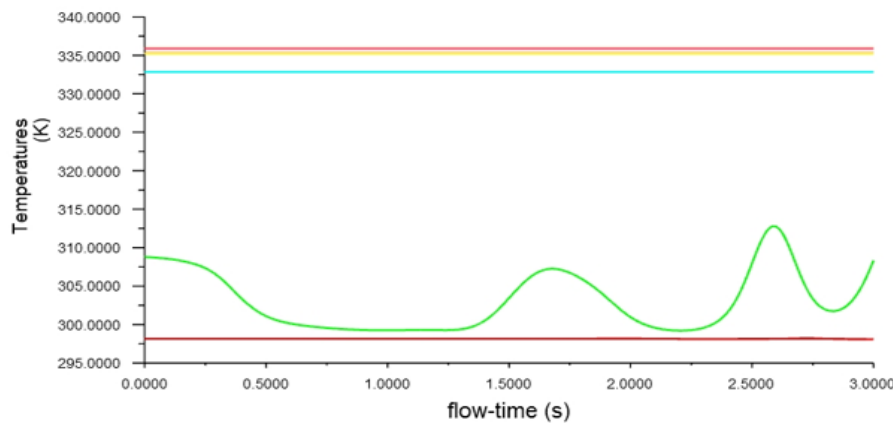


**Figure 35: Temperature residuals of laminar transient simulations**

	Sensor 1 °C	Sensor 2 °C	Sensor 3 °C	Sensor 4 °C	Sensor 5 °C	Ambient Temp. °C
<b>Experimental Data</b>	70.1	69.6	66.3	65.6	57.1	24.6
<b>Ericsson Data</b>	70.2	69.6	66.1	65.4	57.1	-
<b>Numerical Data</b>	68.7	68.4	65.9	65.9	60.7	25

**Table 10: Probe temperature readings for the thermocouples and temperature probes placed around the heat pads as depicted earlier. The inlet velocity is 0 [m/s] and fan speed setting is 0%.**

These temperatures were recorded when the inlet velocity to the numerical model was specified as 0 [m/s] and the fan speed setting for the experiments was 0%. It can be seen that the temperature variations are within a margin of 3[°C], except for sensor 6. Sensor 6 was offset by small distance, moving it closer to the heat pads, recording higher temperatures.

	Sensor 1 °C	Sensor 2 °C	Sensor 3 °C	Sensor 4 °C	Sensor 5 °C	Sensor 6 °C
Experimental Data	60.5	59.7	57.4	56.6	48.8	48.7
Ericsson Data	61.0	60.9	57.8	57.0	50.5	50.3
Numerical Data	62.8	62.6	59.0	59.1	51.6	54.0

Table 11: Probe temperature readings for the thermocouples and temperature probes placed around the heat pads as depicted earlier. The inlet velocity is 1.5 [m/s] and fan speed setting is 50%.

As mentioned in the methodology section, trial and error method was adapted to increase the inlet velocity in the numerical model and match with the temperatures of experimental readings (with different fan speed settings). When the inlet velocity was specified to be 1.5[m/s] and the fan speed setting was 50%, the temperatures matched closely, as presented in **Tab.11**

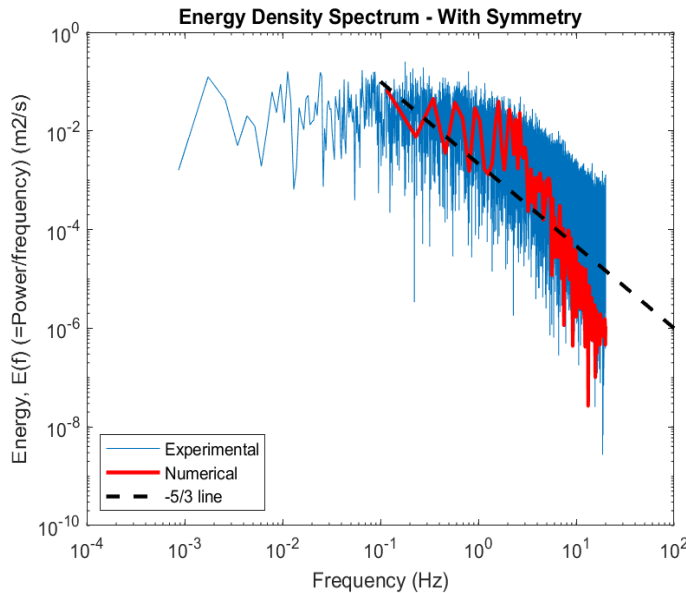
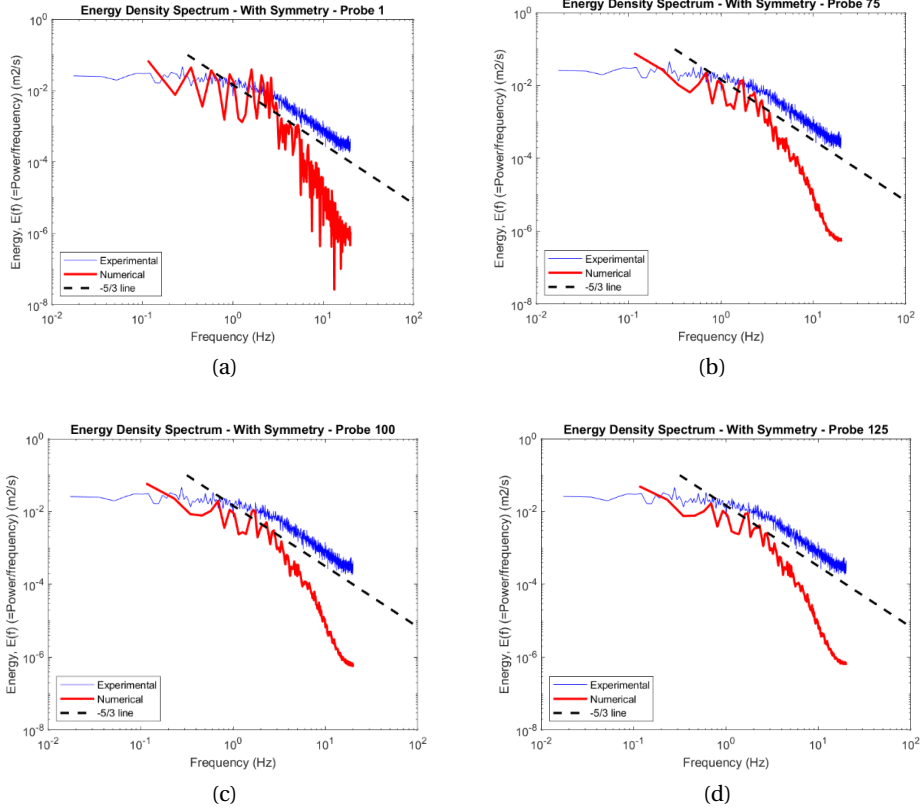


Figure 36: Energy Density Spectrum or the Turbulence spectra for non averaged experimental and numerical data sets

The Energy Density Spectrum comparison for the non averaged numerical and experimental data sets are presented in the **Fig.36**. The black dotted line represents the  $-5/3$  slope line, from the Kolmogorov's hypothesis, explaining the turbulence cascade process. The cumulative averaging process and the windowing concept of averaging for the experimental data set is adapted and the energy density spectra are filtered out. This can be visualised from the **Fig.37**. It can be seen that as the number of probes used in the cumulative averaging process increases, the Energy Density Spectrum curve thins out.

From **Fig.37**, it can be inferred that the red curve (numerical data set curve) in the



**Figure 37: Cumulative averaging of the Energy Density Spectrum, for increasing number of probes used in the averaging process**

energy density plot changes its shape in very small manner after 75 probes (75 Probes indicates the spectra, plotted from averaging of Turbulent Kinetic Energies of 75 probes as a whole). A conclusion can be drawn from this that, the number probes used in the cumulative averaging are sufficient enough. If at all, there were noticeable changes, then a greater number of probes would be required.

The integral length scale values computed using the Eq.19, from Roach's approach is presented in the Tab.12.

	<b>Integral length scale [m]</b>
Experimental data - 50% Fan power	0.052
Numerical data - With symmetry	0.0462

**Table 12: Integral length scales of experimental and numerical data in meters [m]**

The turbulent intensity values computed using the Eq.20, with a characteristic velocity of 0.6 [m/s] is presented in the Tab.13. This value of characteristic velocity is extracted from the experimental data (50% fan power, anemometer located between front door and radio unit), presented in Tab.9. The RMS (Root Mean Squared) value or the standard deviation of the velocity component is calculated for each probe and then turbulent intensities are obtained. Probe 13 matches the fixed position of the anemometer. Other probes are around this fixed location, whose values will be presented in Fig.38 The

variations of turbulent intensity values with probes situated at different locations can be seen in the graph.. As we move away from the fixed position (where the anemometer would actually record the data- Probe 13), the intensity reduces. This is due to the fact that the flow has less interactions with the radio unit and receives cleaner air compared to nearer probes (Probes 1 to 25 located in the first layer) around the fixed position.

	Turbulent intensity [%]
Experimental data - 50% Fan power	17.8
Numerical data - With symmetry	12.9

Table 13: Turbulent intensity of experimental and numerical data in meters [m]

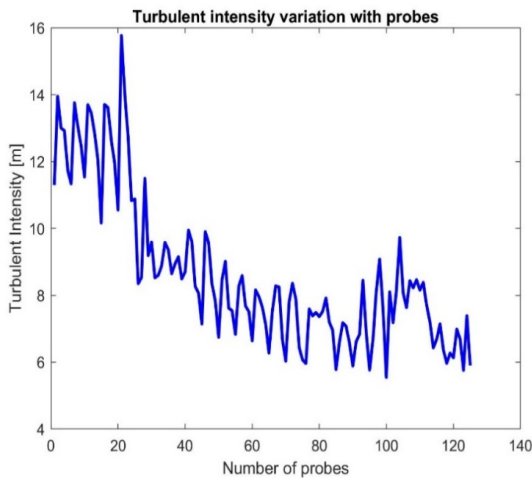


Figure 38: Turbulent Intensity variations for domain with symmetry consideration

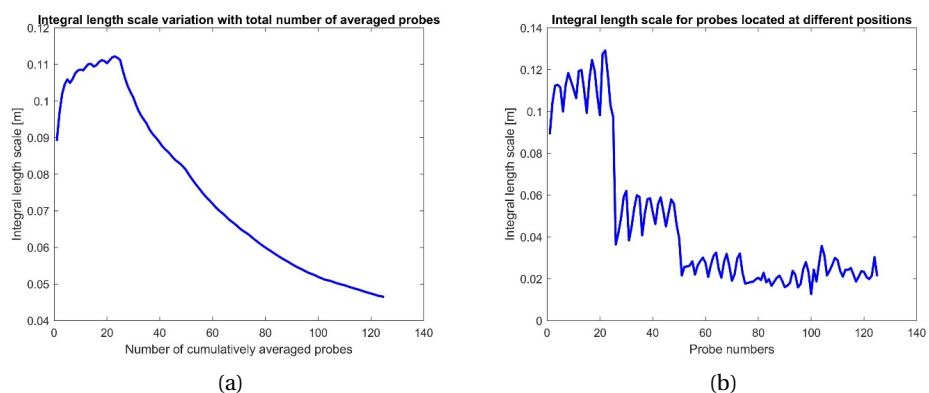


Figure 39: Integral length scale variations for domain with symmetry consideration. The graph in (a) shows the variation in magnitude of integral length scales as the number of probes used for averaging increased. And the graph in (b) indicates the integral length scale values at different locations in the domain, represented by probe numbers

**Fig.39(a)** shows the variation of the integral length scales computed from the numerical data set with the number of probes used to compute the cumulative average. And,

**Fig.39(b)** shows a graph of integral length scale vs probes (probe numbers correspond to different probe locations). Here in the x-axis different probe numbers corresponds to different locations around the anemometer located between the radio and the front door.

First 25 probes lie in the closest proximity for the fixed location, with probe 1 corresponding to topmost left probe. And probe 25 corresponds to bottom right probe. The next 25 probes (Probe 25 to Probe 50) are located 62.5mm apart from the first 25 probes in lateral direction. Similarly 125 different probes are located within a cube of side 250mm. From the graph **Fig.39(b)** it can be seen that the probes nearer to the fixed location have larger length scales and the values decreases as the distance is increased in lateral direction. This can be due to the fact that the probes away from the fixed location receives much cleaner air compared to that of probes in the fixed location. However, a need for sampling velocity data at many locations is required, thereby providing insights about the structures at many locations, and to see if the same trend is followed.

From the turbulence spectra comparison plots in **Fig.40**, the black curve represents half-domain (the domain is split into two equal parts, left and right along the longitudinal plane, considering only the left part). The red curve represents the Energy density spectrum curve for the full domain, without any symmetry consideration.

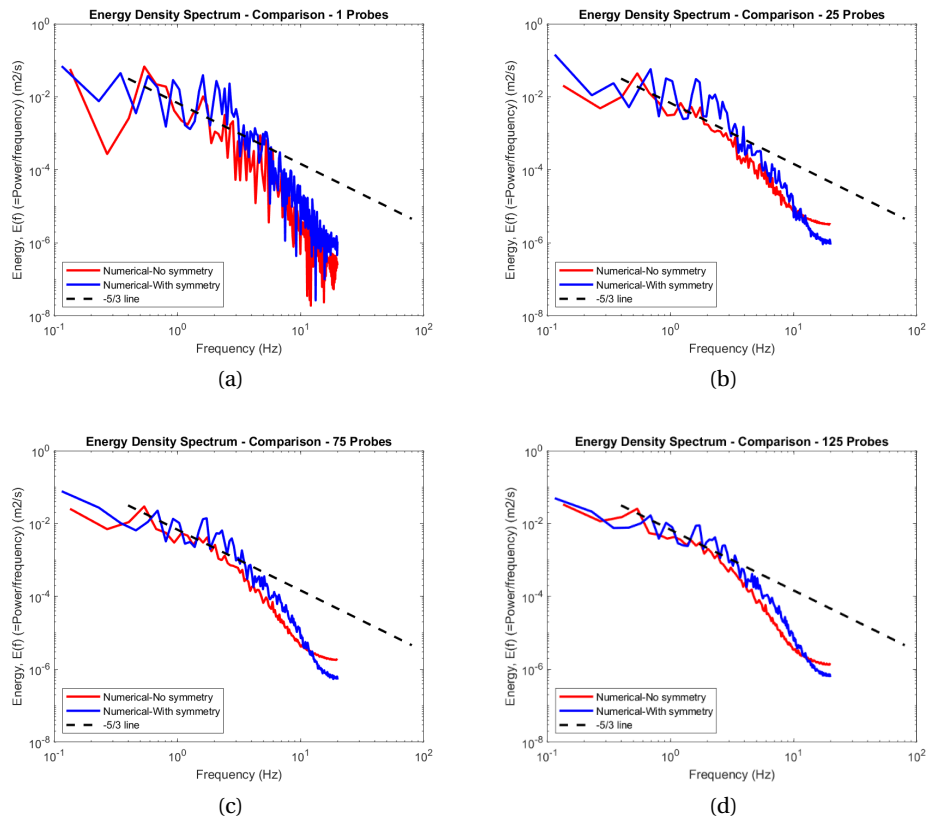


**Figure 40: Comparison of energy density graphs of symmetrical and non-symmetrical domain**

The curves (spectral curves in red and blue colour) are slightly offset from each other. It can be seen that the black curve needs more smoothing, indicating that the data set used for averaging is not sufficient (even though 225 probes are used in the No-symmetry

domain, only 125 probes are used for comparison against the domain which has symmetry consideration).

The probe numbering are quite different than the symmetry case. First 125 probes are placed in the same location as they are placed in the domain where the symmetry condition is considered. Next 100 probes from Probe number 126 to probe number 225 are placed in the consecutive layers in the direction away from the fixed position towards the right wall. Henceforth, a dip in the graph presented in **Fig.41**. The larger the data set, the better the approximation. The averaged value integral length scale for 225 probes is presented in **Tab.14**.

	<b>Integral length scale [m]</b>
Experimental data - 50% Fan power	0.052
Numerical data - With symmetry	0.046
Numerical data - No symmetry	0.039

**Table 14: Integral length scales of Symmetry and No-symmetry consideration domains in meters [m]**

The vortices generation is largely affected by small discrepancies in the geometry generation or the physics specified to the numerical model. The variation of integral length scales in the domain which has no-symmetry consideration is presented in the **Fig.41**

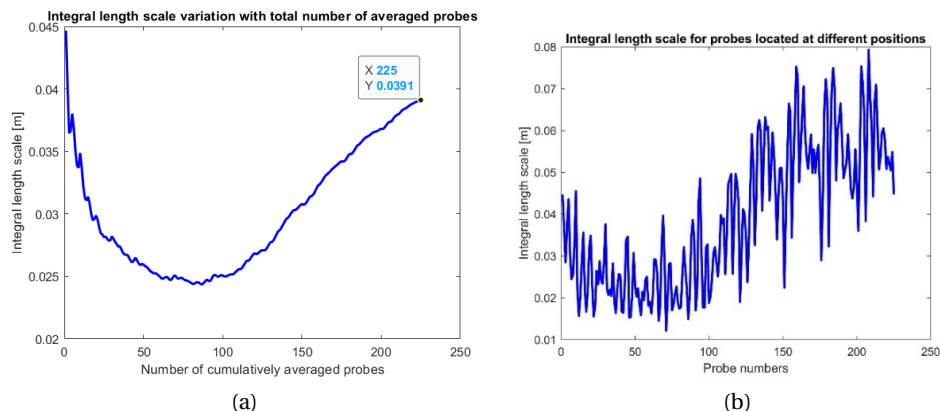


**Figure 41: Integral length scale variations for domain without symmetry consideration. The graph in (a) shows the variation in magnitude of integral length scales as the number of probes used for averaging increased. And the graph in (b) indicates the integral length scale values at different locations in the domain, represented by probe numbers**

The comparison integral length scales between the domain with and without symmetry is collectively presented in the **Fig.42**. It can be inferred that the limited domain (domain with symmetry), has smaller values of integral length scales. A shift in the curves can be seen, although they follow the similar trend. One of many reasons is due to the values of the flux parameters (velocity in particular), along the symmetric plane is specified to be zero, thereby changing the physics generated in two different domains.

**Fig.43** shows the velocity streamlines along the symmetric plane. These contours are for the domain where, the symmetric assumption is considered. Re-circulation zones are seen at the corners of the climate chamber, where there is intensive mixing phenomena happening. Though these streamlines are the representation of averaged values, they

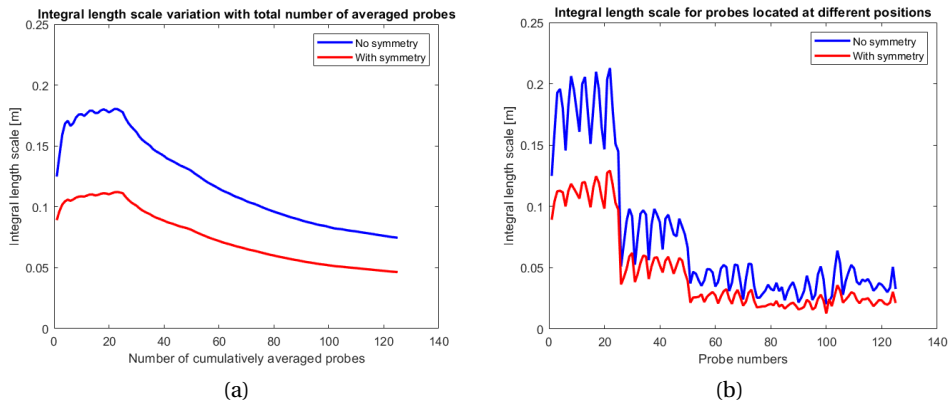


Figure 42: Integral Length scale comparisons b/w the domain with and without symmetry.

depict the flow behaviour. These streamlines are for the time instance of 6 [sec], when the transient run is completed.

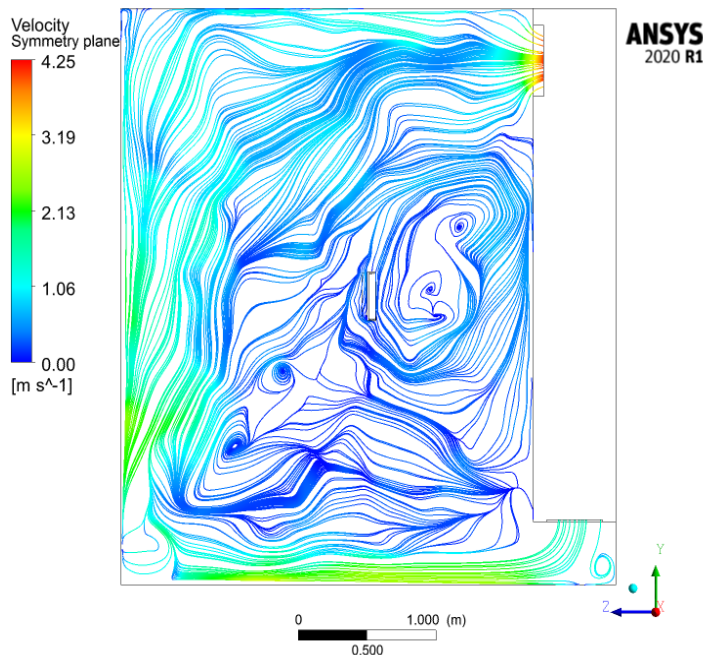
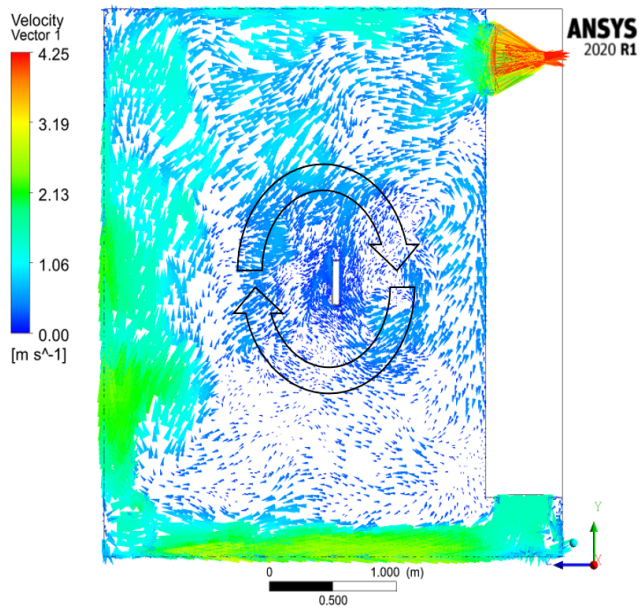


Figure 43: Velocity streamlines along the symmetrical plane of the domain

**Fig.43** presents the vector plots of velocity along the symmetry plane. These vectors indicate the cyclic manner of flow inside the climate chamber. The flow circulates roughly in the clockwise direction within the test space volume. Small recirculation zones can be found in this test space volume, which largely depend on the density variations in the air due to heat transfer.

It can be inferred from the streamlines plot that the velocity of the flow is higher along the walls of the climate chamber, and the flow is relatively slow in the test space volume (volume around the radio unit). This low velocity flow is responsible for the natural convection of the heat from the radio unit to the surrounding air. The heat transfer from the



**Figure 44:** Velocity vectors along the symmetrical plane of the domain

radio unit can be visualized from the temperature contours presented in the **Fig.45.**

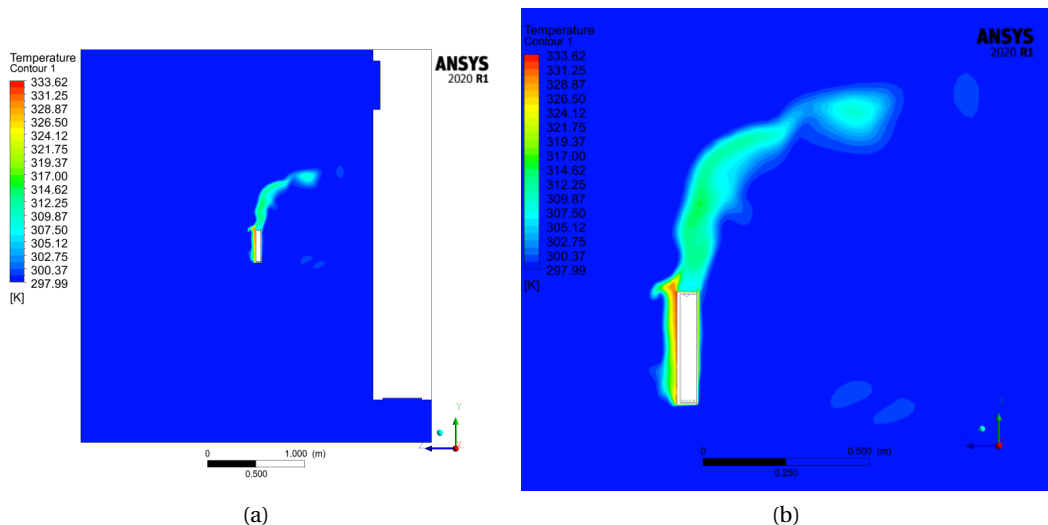


**Figure 45:** Temperature streamlines along symmetrical plane of domain and zoomed in picture

The heat energy flows from the radio unit to the surrounding air (which is in a cyclic flow, directed towards the outlet due to suction) via convection mechanism. The temperature of the air is cooler compared to the radio unit and more denser compared to the air closer to the radio unit. Henceforth, the temperature of the air gradually reduces as the heat air wave rises up, and in turn rise the overall average temperature of the air inside the test space volume in a slower pace.

# 5 Discussion

## 5.1 Numerical simulation setup

Initially, a steady state analysis of heat transfer was intended to be carried out using the basic two-equation RANS models RNG k- $\epsilon$  model. The motto behind using this RANS model is that, RNG k- $\epsilon$  model is used in many works that model the air flow inside a room, involving heat transfer, low turbulence and forced/natural convection (similar works are [41] and [42]). Considering the fact that, the flow inside the climate chamber is of low Reynolds number, (an inlet velocity of 1.5 [m/s]), the effect of turbulence modeling on flow behaviour is weak, thereby ruling out choice of RNG k- $\epsilon$  model. Later, an unsteady or transient case is built up for more accurate modelling and capturing of the physics involved. The unsteady case is necessary as the steady RANS models go blind in predicting the turbulent eddies in the flow. However, unsteady models by their definition or the way they are built, largely fails in the capturing of the eddies to the expected levels, thus making way for higher level analysis. The effects of buoyancy are considered as the natural convection in the flow is dominant.

Numerical model of the climate chamber is built using the commercial CFD package ANSYS Fluent 2020 R1. Input from the experimental calculations made inside the physical climate chamber, such as the integral length scale and the turbulence parameters help in closely emulating the real physics developed in the climate chamber. The turbulence structures present inside the air circulating determines the nature of the natural convection. Henceforth, turbulence modeling of the air present inside the climate chamber is the vital part here. Presence of the centrifugal fans (for re-circulating the air) implies forced convection, it is not the case here. These fans and other mechanical aids are used to generate a natural convection environment, where the buoyancy forces are significant. Heat is convected away from the radio unit under the influence of gravity. Heat transfer modeling done in the CFD software (i.e, the numerical model) should predict results closer to the experimental results that are extracted from specific locations inside the control volume by means of experimental apparatus.

The measurement of velocity of the incoming air from the inlet section inside the climate chamber is a difficult task. The inlet section is about 2.8 [m] long and 0.33 [m] wide. Measuring the average velocities within the area of  $2.8 \times 0.33$  [ $m^2$ ] was not done. But the magnitude of inlet velocity is an important parameter. Henceforth, trial and error basis method were adopted to find out the average velocities as explained earlier. A reasonable assumption of inlet velocity was specified to be 1.5 [m/s], as the temperature readings of the numerical model matched with the experimental temperature readings with a fan power of 50%.

## 5.2 Numerical results and validation

Initially the temperatures result from the thermocouple readings around the heating pads are compared, maintaining the chronological order of the steps in setting up the simulations. Initially, an inlet velocity of 0 [m/s] was specified to the numerical model inlet, and 0% fan speed setting to the physical climate chamber. This was done to check if the specified heat flux boundary conditions were working fine and the placement of

the temperature probes were in the same locations as in the experimental setup. These results are presented in **Tab.10**. It can be seen that the temperature values for the lower probe (Probe 6) mismatch and have the difference of about 5 [°C]. This is mainly due to the error in the position of placement of the probes. Necessary steps were taken to cross check the parameter, however due to the limited availability of the time, and considering the fact that, 5 other probes gave correct readings, the simulations were not repeated.

Later on the turbulence spectra computed from the velocities recorded from the numerical model. Integral length scales and turbulent intensities are then calculated from the same velocities recorded in the numerical model and presented. Energy cascade is one of the important and determining phenomena for the turbulence modeling. The energy density spectrum (EDS) represents this cascade process in a graphical manner. It is a plot of Energy [ $\text{m}^2/\text{s}$ ] vs Frequency [Hz]. In turbulent flow, the EDS will look like an energy cascade diagram. This is because the kinetic energy is handed down from large eddies to progressively smaller eddies in what is known as an energy cascade. As explained earlier, Energy Density Spectrum plot gives an insight into how the energy contained in a signal (here velocity signal) is distributed with the frequency. Here the energy means the turbulence kinetic energy [ $\text{m}^2/\text{s}$ ].

Energy spectral density is a good technique to understand the turbulent flows. But, one has to be careful about the data that is being used to calculate the turbulence spectra. If the data is not sufficiently enough, here it means not enough sampling time, then there are chances where all the information about desired scales (integral scales) is not represented. Having lesser sampling time would lead to incomplete resolution of all the frequencies present in the turbulence spectrum. Lesser sampling times would also lead to addition of unwanted high frequency components which is commonly known as noise. A total sampling time of 18 [s] were chosen based on the mean inlet velocity and the integral time scales from the experimental results. A total sampling time of 18 seconds is also sufficient enough for one flow through inside the test space volume of the climate chamber. But the experimental data set is enormous (in comparison with the numerical data set), which brings out the necessity for filtering or averaging. This is very well explained in the earlier sections of this report.

In case of the anemometer used in the experiments, the sampling frequency is about 20 [Hz]. In the numerical simulations, a time step of 0.005 [s] is used. This gives us the resolving frequency of 200 [Hz]. Though the resolving frequency is 200 [Hz], the data is sampled from the numerical model at a rate of 20 [Hz], thereby making it comparable to the experimental results. The spectral curve in the **Fig.36**, ends at the frequency corresponding to the sampling frequency of 20 [Hz]. It can be seen that there are lots of fluctuations, as the frequency increases in the x-axis. This is clearly the noise being added to the spectral plot and it is highly undesirable for turbulence analysis. To draw conclusions from the spectral energy plot, or the energy representation, the curve has to be smoother and free from large fluctuations. The black dotted line in the plot, is a line with a slope of  $-5/3$  representing  $k^{-5/3}$  in the energy spectrum refers to the inertial range as per Kolmogorov's hypothesis [43]. In this range the energy cascade or transfer occurs from the larger scales (integral scales) injected to the dissipation scales. This hypothesis assumes that, any value of  $k$  in the inertial range, is independent of the local variables such as injected wavenumber and so on [43].

One of the reasons for generating these energy density spectrum plots is to check if the curve representing the turbulence cascade process of handing over kinetic energies

from the larger scales to the smaller scales corresponds to the dotted black line or roughly has the slope of -5/3. The turbulence spectra from the numerical and experimental data sets follow such trend. Another reason is to find out the value of kinetic spectral energy from the graph, when the frequency corresponds to zero [Hz] on the graph. This value of energy is useful in calculating the integral length scale values from the Roachâs approach **Eq.19**.

The turbulent intensities and the integral length scales are computed using **Eq.19** and **Eq.20**. But the averaging of the energy  $Ef_0$ , when the frequency approaches zero varies according to the spectral curve in the energy density plots obtained. The value of the integral length scale shown in the **Table.12**, there is a difference of 13.04%. Considering discrepancies such as modeling assumptions simplifications, solving techniques, errors in recording the actual data, variables used in the formula for calculating the length scales and so on, this difference is considerable. The actual physics inside the physical climate chamber is not 100% represented inside the numerical model. There are many obstacles inside the climate chamber such as the radio mounting stand, metallic arms that hold the anemometer, wires connecting the radio unit to PSU and thermocouple wires. These obstacles lead to breaking down of the vortices generated, when they reach the front anemometer. Henceforth, the vortices recorded are different in the two cases. Larger length scales(Integral Length scales) of the entire turbulent scales present in the flow inside control volume of climate chamber are of major interest, thereby providing less importance to the smaller scales(Kolmogorov scales). Also, the averaging techniques used for the experimental data sets and the numerical data sets that are used to plot the Energy Density Plots are different from which the  $Ef_0$  value is determined, which is a determining factor in the integral length scale formula.

Generally, turbulent intensities are specified at the inlet of the flow domain with the viscosity ratio, when using turbulent models. The difference in the intensity percentage might be due similar discrepancies as explained in the integral length scales part. The flow is very sensitive to obstacles and in the experiments, there were many props used to support the measurements (Radio stand, radio mounting arm, power supply wires, thermocouples, etc.,) which may have influenced the experimental turbulent intensity value. The variation of the turbulent intensity in **Fig.38** is greatly dependent on the position of probes, away from the radio unit. The probes nearer to the radio unit receives air that is highly chaotic after interacting with the complex geometry. As the air moves away from the radio unit, there are no obstacles, hence the chaotic nature of the flow degrades, resulting in lesser turbulence intensities at probes located far away from the radio unit.

### 5.3 Domain symmetry and non-symmetry consideration

Symmetry assumption during the pre-processing stages of the numerical model build, comes with great advantages in terms of reduction of computational cost and complexities developed during the simulations. Symmetry assumption in a domain that is used for turbulence modeling is quite questionable, as explained and debated in similar other works and literature survey [44]. Turbulence by definition is unpredictable, random and chaotic in nature. But, to what extent this analogy holds good is clearly not known. Henceforth, an effort is put in this thesis to understand the pros and cons of using sym-

metry assumption at necessary regions in the domain used for turbulence resolving and modeling is made. However, RANS methods cannot be trusted completely over LES and vice versa. From visual inspection and looking at the dimensions available in the user manual for climate chamber it is evident that the chamber is mirror symmetric along the longitudinal axis when viewed through the front door. Also, the radio unit used as a heat source is also symmetric along the longitudinal axis.

Symmetric boundary condition comes under Neumann boundary conditions, where the gradient or the derivative of the flux parameter is specified along the line or plane of symmetry. Otherwise, in the Dirichlet boundary condition the direct value of the flux parameter is specified. Symmetric boundary condition in Fluent assumes that flux of all quantities along the symmetric plane to be zero. [11] Henceforth, the normal velocity component of the velocity at the symmetric plane is zero. When the symmetry boundary condition is specified, all the flux parameters (velocity, temperature, pressure, etc.,) have same values at equal distance on either side of the symmetric plane. There is no flow of mass or scalar transport of flux across the symmetric plane. Turbulence is quite an interesting and never-ending topic in computational fluid dynamics. Therefore, all possible simplifications and hypothesis need to be adopted to solve the problem with less complexity, and not compromising on the results predicted by the numerical model. Adapting the symmetry boundary condition outweighs the disadvantages with the advantages it provides. To a certain extent the symmetry boundary condition can be considered as a valid choice for the current numerical model of the climate chamber.

## 5.4 Flow behaviour inside the chamber

Considering the capabilities and the available options in the ANSYS Fluent software, visual aids of the behavior of air flow inside the chamber is presented in the form of velocity vectors **Fig.44**, streamlines **Fig.43** and temperature contours **Fig.45**. With the help of these visual aids, a better understanding of the flow pattern inside the chamber can be imagined and understood.

In an actual physical climate chamber the air enters from the inlet, hits the lower ground of the chamber, making a slight bounce and eventually sticking to the floor under the influence of the gravitational forces. The velocity of the flow coming out from the inlet is about 1.5[m/s]. The walls of the climate chamber including the floor are no-slip walls (numerical model is also specified with the same boundary conditions), where viscosity is a major influence on the dynamics of the flow. The air flows throughout the length of climate chamber's floor in cross-sectional direction, developing boundary layer profiles at a distance very close to the wall.

Air flow inside the climate chamber is a closed-circuit flow, as there is no fresh air added or removed from the volume. However, certain leakages when the testing is carried out that are neglected. The mass flow rate of air into the chamber is equal to the mass flow rate out of the chamber, satisfying the law of conservation of mass. The walls of the climate chamber are insulated so that there is no heat transfer by conduction to the outer environment.

As the flow proceeds along the floor of the chamber for about 3.6 [m] the flow slightly loses the kinetic energy in it and hits the front door. This changes the direction vector of the flow, making it to rise along the height of the chamber. Spilling or scattering of the flow occurs, leading to the diffusion phenomena in the test space volume of the climate

chamber as indicated in a cyclic manner in **Fig.44**. Buoyant forces are strong in nature around the radio unit (centre of the test space volume). The buoyant forces or effects of buoyancy are due to the temperature gradients in the flow around the radio unit (heat source), where the heat transfer occurs through convection mechanism.

The convection here is considered as Natural convection as the buoyant effects are dominant and the mean velocity of the flow around the radio unit is much smaller than that of the general forced convection cases. These forces make the fluid to further rise in upward direction, as the denser fluid (cold air) replaces the hotter air. Though, the effects of radiation of the heated radio unit on the air is very small compared to that of convection phenomena **Fig.45**, it is effectively modeled using a radiation model in the numerical model.

Outlets, three ducts with centrifugal exhaust fan in each of them are located close to the ceiling of the climate chamber in the back wall as shown in **Fig.14**. These outlets tend to create suction force, where the air is sucked in as it rises due to the buoyant forces and the inherent kinetic energy. Henceforth the air inside the climate chamber follows a roughly circular path interacting with inlets, radio unit and outlets in a cyclic manner. The velocity of air leaving the test space volume through outlets is comparatively higher than the velocity at the inlets. This is because, the area of inlet is much larger than the three of the outlets all combined.

A flow recirculation or high-pressure areas are generated at the corners of the climate chamber walls. A strong recirculation zone, where the flow velocity is substantially low, is found in the corner closer to the inlet (corner of the back wall and the floor) as seen in the **Fig.43**, that shows the velocity streamlines.

## 6 Conclusions

This report has focused on the initial attempt towards developing a virtual climate chamber. Summarized in this paragraph are the points discussed in the result section. First it starts by showing results for the post processing of the turbulent flow data obtained experimentally and numerically; how the results from the indoor test procedures compare to themselves and how they compare to the predictions made by the model. Although direct comparison of every result obtained from the experimental calculations is not done with the numerical results, vital parameters are covered and suitable reasoning for the same is motivated, these parameters are temperature, turbulence intensity and integral length scales.

Many other variables affect the wind indoors inside the climate chamber, and therefore no clear comparison can be made between numerical and experimental scenarios. The baseline numerical model of the physical walk-in climate chamber built using the commercial CFD software Fluent 2020 R1, emulates the physics inside the test space volume to a reasonable extent. The results predicted by this model are comparable to the experimental indoor results obtained, which follow the same trend and lie in the same range. Main reason for the differences between the experimental and numerical data set is due to the mismatches in the locations where data was sampled. The locations, in terms of height above the floor, and the distance away from the radio unit were not exactly same.

For the purpose of unsteady thermal analysis, the choice of Laminar transient model is satisfactory, as it resolves a large enough part of the spectra, computing a reasonable representation of the flow to build a numerical model of the climate chamber. The physics described between symmetry and non-symmetry cases are different, but more information is required to understand the symmetry consideration i.e. the influence of the velocity component normal to the symmetry plane.

One potential major drawback of this numerical model would be that, this baseline model is entirely dependent on the mesh generated. If a testing unit with different geometry is used, then the whole mesh has to be redone. However, this would be lot easier than actually manufacturing a prototype and manually testing it.

## 7 Future recommendations

- Smaller mounting equipment inside the climate chamber can be preferably used, thereby having least interference effects on the air flow.
- Shorten the distance of the anemometers placement from the radio unit, which would aid in gathering more details about how the airflow around the radio unit is affected by dissipation of heat.
- Improve the understanding of the influence of the geometrical features at the inlet and near the radio unit.
- Explore DES / SAS modeling approach, with more concern towards the buoyancy, and compressibility effects of the flow in the chamber.
- Compare more turbulence parameters between numerical model and experiments such as, isotropy, variance, eddy viscosity, eddy diffusivity and turbulence kinetic energy.
- The choice of the boundary conditions implemented in the model are crude, that uses the default values, bringing a need for more research and reasoning to adapt problem specific boundary and operating conditions.

# References

- [1] Makers FE. How does an Environmental Chamber Work?; 2019. <https://www.dellamarca.it/en/how-does-an-environmental-chamber-work/>.
- [2] Bapat P. Design and fluid simulation of a fluidic growth chamber, Department of IEI, Linköping University; 2019.
- [3] M Bonello SPB D Micallef. Humidity micro-climate characterisation in indoor environments: A benchmark study, University of Malta, Malta; 2019.
- [4] K J Hsieh FSL. Numerical modeling of buoyancy-driven turbulent flows in enclosures, University of Waterloo, Canada; 2003.
- [5] Ruchi Choudary AM. A Methodology for micro-level building thermal analysis: Combining CFD and Experimental set-ups, The University of Michigan, USA; 2001.
- [6] Sadrizadeh S. Numerical study of temperature-controlled airflow in comparison with turbulent mixing and laminar airflow for operating room ventilation, KTH, Stockholm, Sweden,; 2018.
- [7] Limin Wanga GL Lin Zhang. A CFD Simulation of 3D Air Flow and Temperature Variation in Refrigeration Cabinet; 2015.
- [8] Yong Quan MGJK Shuai Wang. Field Measurement of Wind Speeds and Wind- Induced Responses atop the Shanghai World Financial Center under Normal Climate Conditions, Tongji University, Shanghai, China; 2013.
- [9] El-Gabry LA, Thurman DR, Poinsatte PE. Procedure for determining Turbulence length scales using hotwire anemometry, NASA/TM 2014-218403. NASA; 2014.
- [10] Roach PE. The generation of nearly isotropic turbulence by means of grids; 1986.
- [11] Pope SB. Turbulent flows, Cornell University. Cambridge University press; 2005.
- [12] Versteeg, Malalasekera. An Introduction to Computational Fluid Dynamics, A finite volume method. Pearson Education Limited; 2007.
- [13] Gårdhagen R. Turbulent Flow in Constricted Blood Vessels , Quantification of Wall Shear Stress Using Large Eddy Simulation, Linköping university; 2013.
- [14] Jasak H. Turbulence Modelling for CFD, Faculty of Mechanical Engineering and Naval Architecture, University of Zagreb, Croatia; 2017.
- [15] Sagaut P. Turbulence: Dynamics and Modeling, MEC 585, Part-1,DâAlembert Institute,University Pierre et Marie Curie -Paris 6; 2018. <http://www.lmm.jussieu.fr/~sagaut/cours1.pdf>.
- [16] McDonough JM. Introductory lectures on Turbulence-Physics, Mathematics and Modeling, Departments of Mechanical Engineering and Mathematics, University of Kentucky; 2004. <http://web.engr.uky.edu/~acfd/lctr-notes634>.

- [17] Chapman GT, Tobak M. Observations, Theoretical Ideas, and Modeling of Turbulent Flows- Past, Present and Future, in Theoretical Approaches to Turbulence, Dwyer et al; 1985.
- [18] Hu H. Computational Fluid Dynamics, Fluid Mechanics (Fifth Edition), Pages 421-472; 2012. <https://www.sciencedirect.com/science/article/pii/B9780123821003100101>.
- [19] Hereford S. CFD Analysis of Cold Stage Centrifugal Pump for Cooling of Hot Isostatic Press with Validation Case Study, Master's Thesis within Department of Mechanics, KTH University, Stockholm; 2017.
- [20] Saad T. Turbulence modeling for beginners, University of Tennessee Space Institute; 2017. [cfd-online.com/W/images/3/31/Turbulence\\_Modeling\\_For\\_Beginners.pdf](http://cfd-online.com/W/images/3/31/Turbulence_Modeling_For_Beginners.pdf).
- [21] C D Argyropoulos NCM. Recent advances on the numerical modelling of turbulent flows, Department of Chemical Engineering, Imperial College London, South Kensington Campus, London SW7 2AZ, UK; 2015.
- [22] Cinnella P. Recent progress in high-fidelity Computational Fluid Dynamics, DynFluid Laboratory, Arts et Metiers ParisTech, Paris, France and Universita del Salento, Lecce, Italy; 2014. <http://calliope.dem.uniud.it/SEMINARS/ABSTRACT-SEMINARS/Slide-cinnella.pdf>.
- [23] McMurtry P. Turbulence ME 7690, Department of Mechanical Engineering, University of Utah; 2007. <https://my.eng.utah.edu/~mcmurtry/Turbulence/turbmod.pdf>.
- [24] r Aleksey Gerasimov. Quick Guide to Setting Up LES-type Simulations, European Technology Group,ANSYS Sweden AB; 2016.
- [25] Pijush KK, Cohen IM, Dowlin DR. Fluid Mechanics. Elsevier Inc.; 2012.
- [26] Addad Y, Gaitonde U, Laurence D, Rolfo S. Optimal Unstructured Meshing for Large Eddy Simulations, School of Mechanical, Aerospace and Civil Engineering, University of Manchester,Manchester M60 1QD, UK; 2007.
- [27] Davidson L. An Introduction to Turbulence Models,Department of Thermo and Fluid Dynamics, Chalmers University Of Technology, Goteborg, Sweden,; 2018.
- [28] Laney CB. Computational Gasdynamics. 1st ed. Cambridge University Press; Jun.
- [29] Sosnowski1 M, Krzywanski1 J, Gnatowska2 R. Polyhedral meshing as an innovative approach to computational domain discretization of a cyclone in a fluidized bed CLC unit, Czestochowa University of Technology, Faculty of Mechanical Engineering and Computer Science, 21 Armii Krajowej Av, 42-200 Czestochowa, Poland; 1986.
- [30] Ferguson S. Polyhedra: Natureâs Answer to Meshing, SIEMENS CD-adapco,; 2013.

- [31] Marcin Sosnowski KGRG Jaroslaw Krzywanski. Polyhedral meshing in numerical analysis of conjugate heat transfer, University of Technology, Faculty of Mechanical Engineering and Computer Science, 21 Armii Krajowej Av, 42-200 Czestochowa, Poland; 2018.
- [32] NPTEL. Basics of heat transfer, Module 1, NPTEL; 2016.
- [33] Holman J. Heat Transfer, 9th ed., New York: McGraw-Hill; 2002.
- [34] Nahle N. Heat transfer, Biology Cabinet, San Nicolas de los Garza, Nuevo Leon, Mexico.; 2002. [http://www.biocab.org/Heat\\_Transfer.html](http://www.biocab.org/Heat_Transfer.html).
- [35] Bakker A. Heat transfer, Lecture 13, Applied Computational Dynamics, Fluent Inc.; 2002.
- [36] Bahrami M. Natural convection, ENSC 388 (F09), Laboratory for alternative energy consumption, Faculty of Applied Science, Simon Fraser University, Canada; 2015.
- [37] HeatSinkCalculator. The importance of radiation in heat sink design, Heat sink design calculator; 2020. <https://www.heatsinkcalculator.com/blog/the-importance-of-radiation-in-heat-sink-design/>.
- [38] Fluent. Heat transfer modeling, Introductory FLUENT Training, ANSYS Fluent Inc.; 2006.
- [39] Ammar M Abdilghanie LRCDAC. Comparison of Turbulence Modeling Strategies for Indoor Flows, Sibley School of Mechanical Aerospace Engineering, Cornell University, Ithaca, NY 14853-7501; 2009.
- [40] Ivo Dzijan SK Zdravko Virag. Comparison of the SIMPLER and the SIMPLE Algorithm for Solving Navier-Stokes Equations on Collocated Grid, University of Zagreb, ISSN 1333-1124, UDK 519.6: 532.5; 2006.
- [41] Karel Frana MM Jianshun S Zhang. A Numerical Simulation of the Indoor Air Flow, World Academy of Science, Engineering and Technology, International Journal of Mathematical, Computational, Physical, Electrical and Computer Engineering Vol:7, No:6, 2013.
- [42] Huijuan Chen BM. COMPARING k-epsilon MODELS ON PREDICTIONS OF AN IMPINGING JET FOR VENTILATION OF AN OFFICE ROOM, University of Gävle and Linköping university; 2011.
- [43] Glenn Flierl RF. 12.820 Turbulence in the Ocean and Atmosphere. Spring 2007. Massachusetts Institute of Technology: MIT OpenCourseWare; 2006. <https://ocw.mit.edu/courses/earth-atmospheric-and-planetary-sciences/12-820-turbulence-in-the-ocean-and-atmosphere-spring-2007/lecture-notes/ch5.pdf>.
- [44] Guenther S. Symmetry methods for turbulence modeling, Fachgebiet fur Stromungsmechanik und Hydraulik, Technische Universitat Darmstadt; 2005.